Mitigation of Harmonics and Inter-Harmonics with LVRT and HVRT Enhancement in Grid-Connected Wind Energy Systems Using Genetic Algorithm-Optimized PWM and Fuzzy Adaptive PID Control

Abdelkader Mostefa[1], Houari Merabet Boulouiha[1,2], Ahmed Allali[1], Mouloud Denai[3]

[1] *University of Science and Technology Mohamed Boudiaf, Oran, Algeria.*
Faculté de Génie Electrique, Département d'Electrotechnique
LDDEE, Laboratoire de Développement Durable de l'Energie Electrique
[2] *Ecole Normale Polytechnique Oran, ALGERIA,*
[3] *School of Engineering & Computer Science, University of Hertfordshire, Hatfield, UK*

Abstract The growing installed wind capacity over the last decade has led many energy regulators to define specific grid codes for wind energy generation systems connection to the electricity grid. These requirements impose strict laws regarding the Low Voltage Ride Though (LVRT) and High Voltage Ride Though (HVRT) capabilities of wind turbines during voltage disturbances. The main aim of this paper is to propose LVRT and HVRT strategies that allow wind systems to remain connected during severe grid voltage disturbances.

Power quality issues associated with harmonics and inter-harmonics are also discussed and a control scheme for the grid-side converter is proposed to make the Wind Energy Conversion System (WECS) insensitive to external disturbances and parametric variations. The Selective Harmonic Elimination Pulse Width Modulation (SHE-PWM) technique based on Genetic Algorithm optimisation is employed to overcome over-modulation problems, reduce the amplitudes of harmonics and thus reduce the Total Harmonic Distortion (THD) in the current and voltage waveforms. Furthermore, to compensate for the fluctuations of the wind speed due to turbulence at the blades of the turbine, a fuzzy PID (Proportional-Integral-Derivative) controller with adaptive gains is proposed to control the converter on the generator side.

NOMENCLATURE

LVRT	Low Voltage Ride Through
HVRT	High Voltage Ride Through
WECS	Wind Energy Conversion System
SHE-PWM	Selective Harmonic Elimination Pulse Width Modulation
GA	Genetic Algorithm
THD	Total Harmonic Distortion
PID	Proportional-Integral-Derivative
SCIG	Squirrel-Cage Induction Generator
PCC	Point of Common Coupling
PV	Photovoltaic
DFIG	Doubly-Fed Induction Generator
P, Q	Active (P) and reactive (Q) powers of the grid
V	RMS voltage (V) of the grid
FLC	Fuzzy Logic Control
SCSG	Super-Conducting Synchronous Generator
PMSG	Permanent Magnet Synchronous Generators
PSO	Particle Swarm Optimization

DVR	Dynamic Voltage Restorer
MOBA	Multi Objective Bees Algorithm
SPWM	Sinusoidal Pulse Width Modulation
MPPT	Maximum Power Point Tracking
IFOC	Indirect Rotor Flux-Oriented Vector Control
DC	Direct Current
AC	Alternating Current
RSC	Rotor Side Converter
GSC	Grid Side Converter
DSR	Dynamic Serial Resistance
PLL	Phase Locked Loop
SVPWM	Space Vector Pulse Width Modulation

Abreviations

β	Pitch angle of the blades [º]
C_p	Power coefficient
P_m	Mechanical power [W]
T_m	Mechanical torque [N.m]
λ	Tip speed ratio
R	Radius of the turbine [m]
Ω_m	Mechanical speed of the turbine [rad/s]
v	Wind speed [m/s]
ρ	Density area [kg.m^{-2}]
i_{gd}, i_{gq}	Active and reactive Park components of the grid [A]
V_{GN}	Normalized grid voltage at the PCC [p.u]
I_N	Nominal current of the wind system [A]
i_m	Grid current [A]
v_{dc}	DC link voltage [V]
v_{dcref}	DC link reference voltage [V]
V_{LL}	Line-to-line voltage of the grid [V]
m_i	Modulation index
δ	Phase shift between the fundamental voltage the converter and voltage of the grid [rad]
i_{gref}	Reference current of the grid [A]
Δ	Variation symbol
ω_e	Grid angular frequency [rad/s]
v_d , v_q	Voltages of the grid Park [V]
v_{od} , v_{oq}	Inverter voltage components [V]
v_{odref} , v_{oqref}	Inverter reference voltage components [V]
t	Is the time [s]
R_f, L_f	Leakages resistance [Ω] and inductance [H] of the transformer
C	Capacitor of the DC bus [F]
a_n , b_n	Coefficients of Fourier series decomposition
K	Number of switching angles
$\alpha_1, \alpha_2, \dots, \alpha_K$	Switching angles [º]
$\varepsilon_1, \varepsilon_2, \dots, \varepsilon_K$	Normalised harmonic amplitude to be eliminated
$f(\alpha_i)$	Cost function or the objective function
FF_v	Fitness function
X	Parameter vector of the objective function
ϕ_{rd} , ϕ_{rq}	Rotor fluxes of d-q axis in the transform of Park [Wb]
v_{sd} , v_{sq}	Stator voltages of d-q axis in the transform of Park [V]
R_s , L_s	Resistance [Ω] and inductance [H] of the stator generator
R_r , L_r	Resistance [Ω] and inductance [H] of the rotor generator
L_m	Cyclic mutual inductance [H]
σ	Coefficient of Blondel

ω_s	Stator speed of the generator [rad/s]
ω_{slip}	Slip speed of the generator [rad/s]
T_r , T_e	Turbine torque and electromagnetic torque [N.m]
p	Number of pole pairs
i_{sd} , i_{sq}	Direct and quadratic stator currents of the generator in the Park frame [A]
Ω_r	Angular rotor speed of generator [rad/s]
k	Discrete time
γ	Self-adjusting gain
$u(t)$	Control signal
$e(t), de(t)$	Error and variation of the error
Kp, Ki , Kd	Proportional, integrator and derivative gains
k_{pmax} , k_{pmin}	Maximum and minimum limits of the proportional gain
k_{dmax} , k_{dmin}	Maximum and minimum limits of the derivative gain
μ	Integral gain adjustment coefficient
k'_p	Normalized value of the proportional action
k'_i	Normalized value of the integral action
k'_d	Normalized value of the derivative action
n	is the order of harmonic
i_g	is the amplitude of the grid current in the Park frame [A]
i_{gn}	is the nominal amplitude of the grid current in the Park frame [A]
K_c	is the controller gain of LVRT and HVRT strategies
f_e	is the grid frequency [Hz]
$D=\frac{\sqrt{v_{od}^2+v_{oq}^2}}{v_{dc}}$	is defined as the ratio between the fundamental of the output voltage and the DC voltage (v_{dc})
I_{dc_gen}	Is the DC current for generator side
ϕ_r	Is the oriented rotor flux [Wb]
A and B	are arbitrary constants matrices
i and j	Are respectively the indices of the counters of the switching angles and of the order of harmonics
v_{abcref}	Three-phase reference voltages of the grid [V]
v_{abc}	Three-phase voltages of the grid [V]
v_a	Is the voltage of phase A of the grid
i_{abc}	Three-phase current of the grid [A]
i_{sabc}	Three-phase current of the generator [A]
i_{gdref}, i_{gqref}	Grid currents references of d-q axis in the transform of Park [A]
v_{d1ref} and v_{q1ref}	Are the output voltages of the regulators [V]
$v_{sabcref}$	Three-phase reference voltages of the generator [V]
v_{sdref} and v_{sqref}	Stator voltages references of d-q axis in the transform of Park [V]
S_{gabc}	States switch of the generator side converter

Keywords Wind energy, power quality, LVRT, HVRT, selective harmonic elimination PWM, genetic algorithm.

1 INTRODUCTION

The world, today, is facing a rapid growth in energy demand (a 50% increase in global energy demand is expected by 2030) [1], rising energy prices (the price of a barrel of oil oscillates around \$50-80), decline in fossil fuel resources (more than 60 oil-producing countries have already exceeded their peaks in production). Moreover, strong regulations on greenhouse gas emissions are gradually implemented, forcing states to change their energy policy and shift to renewable energy sources. Natural resources such as solar, wind, tidal, hydraulic, etc. can generate clean, sustainable and inexhaustible energy and are environmentally friendly. Among these, wind energy is currently the fastest growing source of renewable energy in the world [2,3].

Variable-speed WECS have been designed with different generator topologies and the Squirrel-Cage Induction Generator (SCIG) is amongst the most widely used machine in wind turbine configurations.

The SCIG-based WECS is required to remain insensitive to external disturbances and parametric variations and hence an effective control strategy should be designed to achieve this. Indeed, there is a plethora of control methods which have been proposed in the literature. However, the capabilities of the SCIG-based WECS to mitigate energy quality issues such as harmonic attenuation, reactive power support and voltage swing have not been fully explored. The main contribution of this paper is to investigate these power quality aspects and enhance the controllability of the WECS. These new features are provided by a power converter interfacing the wind generator to the grid. In addition, the reactive power supplied to the grid must be zero to maintain a unity power factor.

The major concerns with the connection of renewable energy sources to the power grid at the Point of Common Coupling (PCC) are associated with the LVRT grid code requirement during grid faults such as [4]: (i) rising of the voltage which causes overcurrent and overheating in the generator and aerodynamic forces of short duration. All these problems lead to fatigue and long-term damage of the equipment. (ii) increase in the losses or an alteration in the energy supply schedule which subsequently lead to a deterioration and shutdown of the system.

With the increasing penetration of wind energy systems into the grid, many countries have imposed new regulations and technical requirements. One of these technical requirements is the so-called LVRT capability which requires wind turbines to remain connected to the grid and continue to supply power under grid voltage disturbances. Several solutions have been proposed to address these problems [5-12]. In [5], a new power control method is developed to improve the system efficiency during fault conditions in the grid. Filter design and the development of advanced synchronization methods for grid-connected Photovoltaic (PV) systems are discussed in [6]. In [7-8], the authors proposed an LVRT technique based on the ANFIS (Adaptive Network Fuzzy Inference-System) for the protection and control of wind turbines.

A control strategy combining sliding mode control and fuzzy logic control for a grid-connected doubly fed induction generator (DFIG) was proposed in [9]. This technique is robust and effective in attenuating grid voltage during faults. The authors in [10] proposed a modified technique for LVRT strategy. This study focused on minimizing overload on the rotor of the DFIG and the voltage variations of the intermediate circuit by modifying the converter control structure of the generator. This approach resulted in a substantial reduction in the electromagnetic torque oscillations during faults. In [11] the authors proposed a DVR (Dynamic Voltage Restorer) based on a cascade multilevel inverter to increase capacity and reduce harmonics in both LVRT and HVRT strategies. The DVR control system is equipped with an optimal fractional $PI^{\lambda}D^{\mu}$ regulator based on the Multi Objective Bees Algorithm (MOBA). The control of the network-side converter can be modified to mitigate the effects of unbalanced voltage. In [12], an analysis of different power control methods of LVRT strategy is presented to minimize the effects of ripples on the network powers and on the DC bus voltage during voltage drops.

A high voltage control method (HVRT) with a P-Q coordination for the DFIG (Doubly-Fed Induction Generator) based on a Q-V control has been proposed in [13]. In the proposed strategy, the reactive power limit of the DFIG can be extended during the transient period in coordination with the DFIG rapid active power control, so that the surge voltage caused by DC bipolar block can be effectively suppressed.

In addition, power electronic converters are usually controlled by PWM strategies and the most popular and widely used PWM techniques are the triangular-sine and hysteresis PWMs which tend to generate more harmonics. To reduce the THD, the switching frequency is usually increased which results in an increase in losses and heating of the switches. To overcome these problems, this paper proposes to use the emerging SHE-PWM method optimized by genetic algorithm (GA) to reduce the THD level. The programmed PWM generates high quality output spectra, which in turn leads to minimal current ripple, thus meeting several performance criteria and contributing to the improvement of the overall system performance.

Because of the nonlinearity of Fourier series equations for the SHE-PWM technique, iterative methods such as Newton-Raphson are employed to solve the system of equations. Alternative numerical methods mainly depend on the initial conditions and divergence problems are likely to occur. GA optimization can be used to solve these equations, without extensive derivation of analytic expressions [14]. SHE-PWM is a very effective method for controlling two-level inverters to improve the quality of their output voltages. It consists in forming the inverter output waveform as a succession of variable width slots. Generally, using a waveform which has a double symmetry with respect to the quarter and to the half period.

The mathematical model of the WECS is complex and non-linear with a strong coupling between the input, output and internal variables. In addition, there are several disturbances, which can affect the performance of the wind energy system such as fluctuations in the wind speed due to air turbulence, uncertainties and parametric variations (like the variation of the stator or rotor resistances as well as the transformer).

In the last years, there has an extensive work to design high performance control schemes for WECS. In [15], the authors proposed a combination of a pole placement of the polynomial regulator RST and Fuzzy Logic Control (FLC) to regulate the real and reactive powers generated by the DFIG. RST controller parameters are adjusted online via an adaptive strategy. In [16], an adaptive fuzzy control method with GA was used for the scheduling of energy resources in a microgrid model. In [17], an adaptive neural PID controller based on the Delta learning mechanism is proposed for speed control of a SCSG (Super-Conducting Synchronous Generator) based WECS. The results of the simulations showed that the proposed control approach has better robustness and stability as compared to the conventional PID controller. In [18], a new adaptive neural PID hybrid control approach for the Permanent Magnet Synchronous Generators (PMSG) based variable speed system has been proposed. In [19], an optimal gain scheduling controller is applied to a variable speed wind turbine to control the power when the wind speed is greater than the nominal value. However, the Optimal Gain Planning Controller cannot be used to exploit maximum wind power from wind speeds below the rated speed, and it is difficult to measure or obtain wind data. The dynamic accuracy the controller has not been considered. In [20], a dynamic programming approach using hybrid fuzzy-adaptive genetic algorithms was used to perform smart grid energy resource planning. A multi-objective linear programming model was developed in [21]. The optimization methods based on the evolutionary algorithms for calculating the switching angles are proposed in [22]. In [23, 24], the authors proposed a modified Particle Swarm Optimization (PSO) algorithm. The developed SPWM over-modulation approach is suggested in [25] for the elimination of the third harmonics in a single-phase inverter.

A high-performance control system generally requires a good transient and steady-state responses and must be insensitive to variations in operating conditions and plant's parameters. Conventional control techniques, such as PI and PID have been widely used in industry [26] but require retuning when the operating point changes. Control techniques based on artificial intelligence methods, on the other hand, have a strong ability to control non-linear systems, handle imprecise parameters, and derive objective decisions by approximate knowledge, even with the change of process operating point [27]. The integration of fuzzy logic with classical adaptive control is also an attractive solution [28].

This paper proposes a control scheme for the wind energy conversion system based on an adaptive PID regulator. Furthermore, a PWM technique with harmonic elimination in the over-modulation region using GA optimization technique is proposed to increase the margin of stability and to improve energy quality.

In summary, this contribution focuses on two main parts: The first part is dedicated to the design of the SHE-PWM technique to reduce additional harmonics created by large voltage drops during the LVRT mode and to ensure a large margin of stability by over-modulation of SHE-PWM technique in HVRT mode. The second part deals with the design of an adaptive fuzzy-PID control scheme for the generator side. This control approach is very effective against external and internal disturbances on the generator side. The proposed control scheme combining SHE-PWM and fuzzy-PID control is used to reduce fluctuations in the DC bus (SHE-PWM is used to attenuate ripples during grid voltage drops and overvoltage and fuzzy-PID is used to reduce fluctuations caused by sudden variations of the grid voltage magnitude and turbulence effects of the turbine in the generator side.

The remaining of the paper is organized as follows: Section 2 describes the configuration and presents the modeling of the wind energy conversion system based on the SCIG generator. Section 3 presents the different control strategies of wind turbines to achieve the LVRT capability with a state of the art on the work done to reduce the problems of grid faults. The proposed new control scheme is also presented in this section. In Section 4, the grid side control system is presented. Section 4 presents the derivation and resolution of the objective function for the SHE-PWM technique based on GA optimization.

The maximum power point tracking (MPPT) for extracting optimal power and the indirect rotor flux-oriented vector control (IFOC) techniques are presented in Section 5. The proposed adaptive PID controller based on fuzzy logic is also derived in Section 5. Section 6 of the paper presents a series of simulation scenarios to evaluate the proposed control design scheme. Finally, the conclusions of this work are summarized in Section 7.

2 STRUCTURE OF THE WIND ENERGY CONVERSION SYSTEM

The WECS shown in Fig. 1 consists of a wind turbine with three (3) blades of radius R connected to a variable-speed SCIG and two converters AC/DC/AC. The first converter is connected on the machine side and is used as a PWM rectifier. The second converter is connected to the grid-side and regulates the voltage of the DC side capacitor and controls the real and reactive powers of the system. The DC bus voltage must be regulated to its reference to ensure power flow between the SCIG and the grid.

SCIG generators connected to the grid through an AC/DC/AC converter can tolerate disturbances and rapid voltage dips.

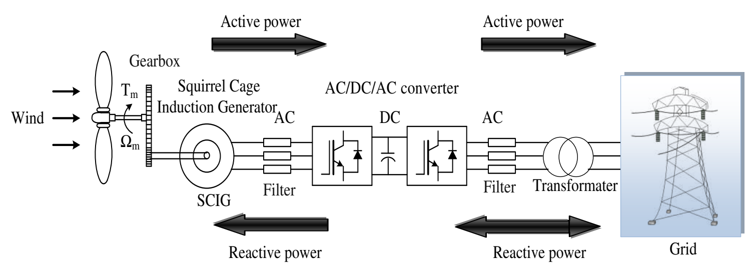

Fig.1 Grid-connected SCIG-based WECS.

The mechanical power of the turbine is given by [29]:

$$P_m = \frac{1}{2}\pi\rho C_p(\lambda,\beta)R^2v^3 \tag{1}$$

Where β [°] is the pitch angle of the blades, C_p represents the power coefficient and describes the aerodynamic effectiveness of the wind turbine. C_p, is a function of speed ratio λ and the pitch angle β of the blade and is given by the following equation [30]:

$$C_p(\lambda,\beta) = 0.5\left[\frac{33}{\lambda_i} - 0.2\beta - 0.4\right]e^{-\frac{12.7}{\lambda_i}} \quad (2)$$

$$\frac{1}{\lambda_i} = \frac{1}{\lambda + 0.08\beta} - \frac{0.035}{\beta^3 + 1} \quad (3)$$

$$\lambda = \frac{\Omega_m R}{v} \quad (4)$$

In equation (4), Ω_m [rad/s] represents the mechanical speed of the turbine.

3 CONTROL APPROACHES FOR WIND ENERGY CONVERSION SYSTEMS UNDER FAULT CONDITIONS

Reactive energy consumption of the wind energy system generally increases with the actual power output unless reactive support ancillary equipment is installed. In the absence of appropriate reactive power compensation, there may be significant variations in the grid voltage, which can cause serious damage to expensive equipment of the transmission grid. To maintain power system stability, utilities often require that the deployment of additional wind farms should not deteriorate the performance of the system or violate the stability criteria. The main objective of this work is to propose an LVRT strategy that will allow the wind generation system to stay connected to the grid and inject power under fault conditions. Fig. 2 summarizes the existing control strategies for different faults.

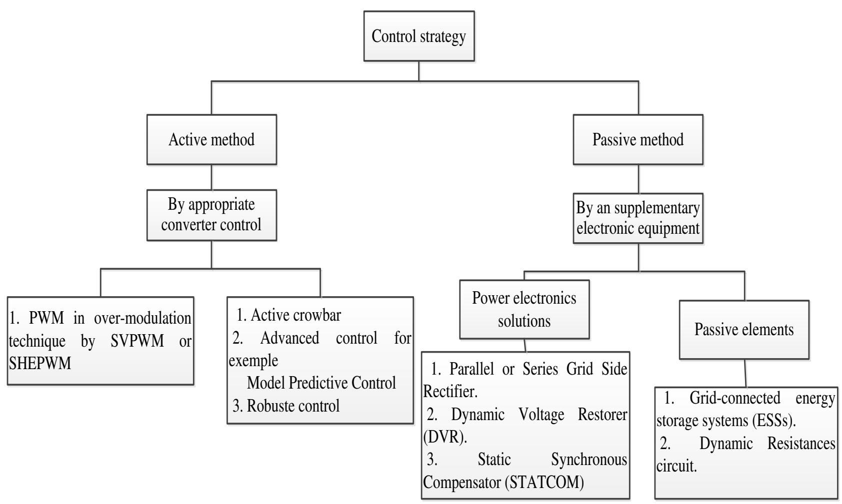

Fig. 2 Control strategies to mitigate grid faults.

Several works in the literature have studied the LVRT capability of the DFIG under voltage dips. When using active crowbar, during voltage dips, the control of the machine side converter (RSC: Rotor Side Converter) is lost and the generator behaves like a SCIG machine [31]. The energy storage system in the DC bus is analyzed in [32], however, the cost and size of the capacitor battery or super capacitor must be considered. In [33], the authors proposed a passive crowbar placed in series with the stator circuit and an active compensator but the control of the (Grid Side Converter) GSC-side converter and the behavior of the DC bus during the fault are not been discussed. A combination of a crowbar and a Dynamic Series Resistor (DSR) was proposed in [34]. A control algorithm based on the use of the energy storage as inertial energy in the rotor during voltage dips is discussed in [35]. An approach based on the demagnetization of the machine to reduce the intensity of the rotor currents is studied in [36]. In [37], the authors propose a combined LVRT and HVRT strategy to improve the dynamic behavior of an unbalanced grid.

However, all these LVRT control strategies increase the equipment size or complexity of the control circuits. In this paper, a new control strategy based on over-modulation has been proposed to increase the system stability margin and regulate the DC bus voltage.

Only a few studies on HVRT technology have been carried out so far [38-41]. A combined protection strategy to avoid disconnection of a wind turbine due to high voltage is proposed in [38]. An efficient HVRT method against high voltages has been proposed in [39]. This strategy is used to provide reactive power to ensure that the DFIG wind turbine operates normally in the event of overvoltage, but the chopper must be used on the DC side of the converter [39]. A rotor excitation control strategy based on variable damping and conditional impedance is proposed in [40] to decrease the electromagnetic torque oscillations during voltage swell and improves the HVRT capability. The authors in [41] proposed a dynamic HVRT control strategy based on the reactive power of DFIG wind turbines. Protection strategies are mainly based on physical protection devices. In fact, the maximum variation of the voltage amplitude is less than 30% of the nominal voltage, so the electromagnetic transient power caused by the voltage variation cannot trigger the protection device.

3.3 Requirements of the low and high voltage ride though and high voltage ride though

The concepts of LVRT and HVRT strategies allow wind turbines, during symmetric and asymmetric faults, to remain connected to the grid and even contribute to the restoration of the grid voltage without loss of controllability of the two AC/DC/AC converters. Fig. 3 represents the standards of the Spanish grid codes for both LVRT and HVRT strategies [42, 43].

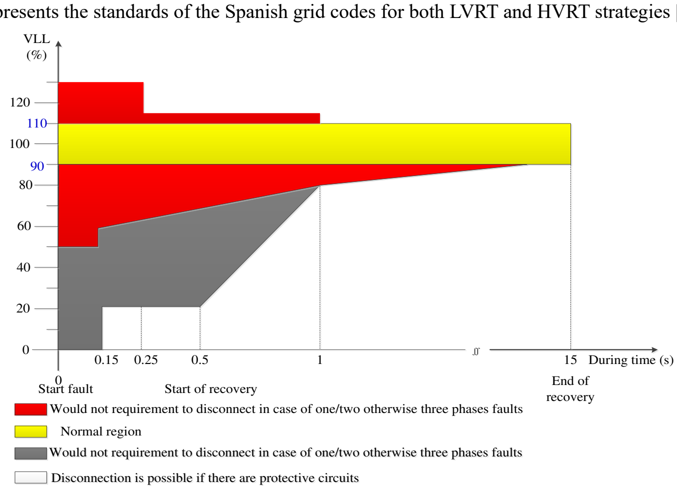

Fig. 3 LVRT and HVRT requirement for the Spanish grid code [42, 43].

In the yellow and red zones, the production system should remain connected to the grid during single, two or three phases faults.

In the grey area, disconnection is not allowed for single and three phase faults. Changes in amplitude of the grid voltage cause either injection of reactive power in the case of HVRT or demand of reactive power in the case LVRT. All control strategies used in the literature have focused on the compensation of reactive currents for voltage support during grid faults. In this work, the grid-side converter is used as a static compensator to produce or consume reactive power to achieve a unity power factor.

a) Requirement of low voltage ride though

The LVRT strategy requires that the wind power generation system should have the capability to connect to the grid when the voltage at the PCC drops after 0.15 sec following a grid fault. The wind system must provide reactive power and the reactive current i_{gq} must meet the following requirements:

$$\begin{cases} i_{gq} \geq 1.5(0.9 - V_{GN})I_N & 0.2 \leq V_{GN} \leq 0.9 \\ i_{gq} \geq 1.5\, I_N & V_{GN} < 0.2 \\ i_{gq} = 0 & V_{GN} > 0.9 \end{cases} \tag{5}$$

Where V_{GN} is the normalized grid voltage at the PCC (in per unit) and I_N is the nominal current of the wind system.

In addition, the grid currents in the Park reference frame must satisfy the following condition:

$$i_m \geq \sqrt{i_{gd}^2 + i_{gq}^2} \tag{6}$$

b) Requirement of high voltage ride though

In addition to voltage dips, voltage swells can also occur in three-phase systems due to grid faults. Thus, for HVRT codes, wind systems must resist to changes in the voltage amplitude for a short period and at the same time absorb some reactive power to enhance the stability of the system. Fig. 3 shows the HVRT requirements for the Spanish national grid. If the voltage at the PCC reaches 130 % of its normal value, the wind system should remain connected to the grid for 0.25 s. On the other hand, during HVRT operation, the wind system should absorb reactive power in order to attenuate the increase in the voltage at the PCC. The Spanish grid code requires that approximately 0.73 p.u. of reactive current should be absorbed when the voltage increases by 130 %.

3.4 Proposed approach for low voltage ride though and high voltage ride though

In this approach, the over-modulation of the PWM technique optimized by GA is used to simultaneously attenuate the amplitudes of harmonics and eliminate the effect of grid voltage imbalances. The principle of this approach is to control the DC bus voltage to achieve a wider range of stability by adjusting the modulation index. Thus, the fault current can be significantly reduced with this control strategy. With reference to Fig. 4, the grid current variation of the LVRT and HVRT strategy is written as $\Delta i_g = K_c.\Delta V_{LL}$ where ΔV_{LL} denotes the grid line-to-line voltage and K_c is defined as the proportionality constant between the current and the voltage which is adjusted by the national grid control center and is in the range $0 < K_c < 10$.

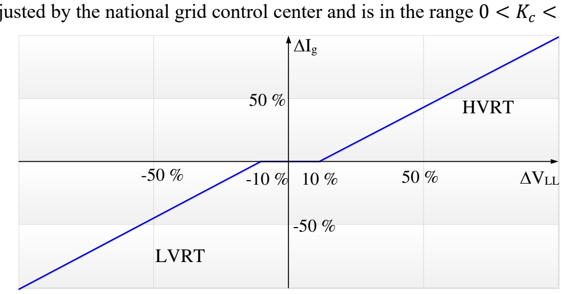

Fig. 4 Reactive current during faults.

The relation between the effective grid voltage and the DC bus voltage is given by $v_{dc} = 2V_{LL}/\sqrt{3}m_i$ where V_{LL} is the line-to-line voltage of the grid. Grid voltage faults are generated in the DC-link. The stabilization of the DC bus voltage is generally achieved via LVRT and HVRT control strategies to ensure smooth operation. However, as stated above, these strategies lead to an increase in the size of the equipment and complexity of its control. In this work, a new control strategy for the DC bus voltage is proposed which provides a wider range of stability without any added equipment.

The variation of the grid voltage influences the fundamental amplitude of the output voltage of the grid-side converter. This can increase the amplitude of the modulation index m_i near the non-linear region of the PWM technique. In the proposed strategy, a SHE-PWM technique with a modulation index that can vary between 0 and 2 is employed to ensure a good stability of the DC voltage and consequently continuity of wind power generation during faults is ensured.

Grid codes have been introduced to ensure (i) reliability and stability of the electricity grid, (ii) continuous and improved quality of service for consumers connected to the grid, (iii) protection of grid assets, and (iv) security and safety of the personnel.

a) Low voltage ride though strategy

The aim of the proposed control strategy for the wind system is to satisfy the LVRT requirement while maintaining a unity power factor in the event of a grid faults. The current reference during network voltage drops is given by:

$$i_{gref} = i_g - \Delta i_g \tag{7}$$

The difference between the current before and after the fault is $\Delta i_g = K_c . \Delta V_{LL}$ where K_c is defined as the proportionality constant between the current and the voltage which is adjusted by the national grid control center and is in the range $0 < K_c < 10$. The network current reference is zero for voltage drops less than -10% of V_{LL}.

b) High voltage ride though strategy

During grid overvoltage, the grid side converter must absorb reactive power to guarantee a unity power factor. For this, the reference current must be equal to:

$$i_{gref} = i_g + \Delta i_g \tag{8}$$

The acceptable tolerance designed for the absorbed reactive power is $\Delta i_g = +20\%\, I_{gn}$. To stabilize the voltage across the power grid during symmetrical and asymmetrical faults, the grid-side converter must absorb the supplementary reactive current. Similarly, the grid current reference is zero for the HVRT technique for voltage drops less than $+10\%$ of V_{LL}.

4. GRID-SIDE CONVERTER CONTROL SCHEME

Fig. 5 depicts the control scheme of the DC bus voltage and Park currents components on the source side. It consists of a three-phase source and a transformer (represented by inductances of leakage resistances), a voltage source inverter and a DC link. The real power is controlled by the direct current component i_{gd} of the source-side converter and the reactive power is determined by the change of the quadratic current component i_{gq}. of the converter.

The Park model is given by the following equation:

$$\frac{d}{dt}\begin{bmatrix} i_{gd} \\ i_{gq} \end{bmatrix} = \begin{bmatrix} -\frac{R_f}{L_f} & \omega_e \\ -\omega_e & -\frac{R_f}{L_f} \end{bmatrix}\begin{bmatrix} i_{gd} \\ i_{gq} \end{bmatrix} + \frac{1}{L_f}\begin{bmatrix} v_d - v_{od} \\ v_q - v_{oq} \end{bmatrix} \tag{9}$$

Where ω_e is the grid angular frequency, v_d and v_q are the Park components of the source voltage, v_{od} and v_{oq} represent the Park components of the inverter voltage, R_f is the leakage resistance of the transformer, L_f is the leakage inductance of the transformer and C is the capacitor of the DC bus. The control system consists of two control loops: An outer loop with a PI controller to regulate the DC link voltage. The DC voltage controller generates the d-axis reference current i_{gdref} of the source which is compared to the measured current i_{gd}.

The q-axis component i_{gq} of the source current controls the reactive power flow. To achieve a power factor of unity i_{gq} is set to zero. The source-side converter controls the level of the capacitor voltage on the DC side and the real and reactive powers of the grid by controlling the modulation index m_i and the phase shift between the fundamental voltage the converter and the grid voltage is denoted by δ.

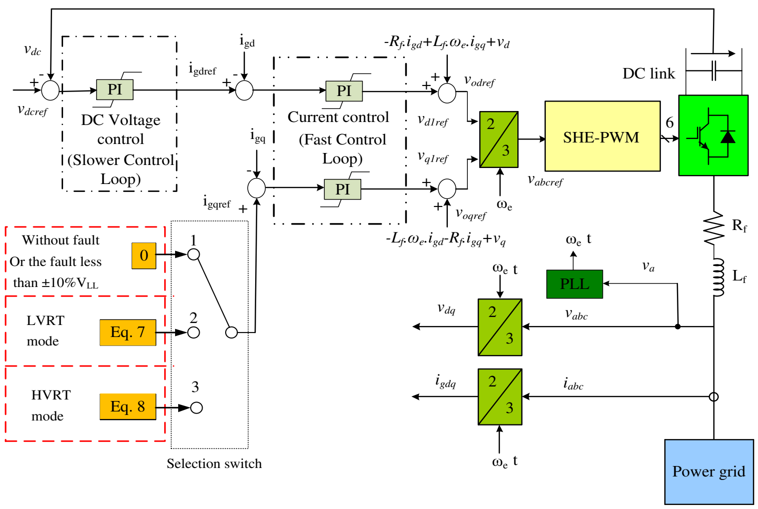

Fig. 5 Control system for the DC link and grid-side.

With reference to Fig. 5, there are three modes of operation:

- ✓ **Mode 1 (switch position 1)**: This is the activation mode for the fault-free case or when the variation of the voltage at the PCC is small.
- ✓ **Mode 2 (switch in position 2)**: This is the activation mode used for the LVRT strategy. In this mode, the grid-side converter produces reactive energy to the grid to achieve a unity power factor.
- ✓ **Mode 3 (switch in position 3)**: This is the activation mode used for the HVRT strategy. In this mode, the line side converter absorbs additional reactive energy.

4.1 Selective harmonic elimination pulse width modulation strategy optimized by genetic algorithm

The SHE-PWM strategy calculates the instants of switching of the inverter switches to satisfy certain criteria concerning the frequency spectrum of the resultant waveform. These sequences are then stored and retrieved cyclically to control the switches. The following criteria are employed: (i) Elimination of harmonics of specified rank. (ii) Elimination of harmonics in a specified frequency band.

In programmed PWM techniques, an objective function is usually selected to optimize the switching instants. One such objective function is the Selective Harmonic Elimination (SHE). The gradient descent and Newton-Raphson methods are traditionally employed to solve this optimization problem. These methods tend to require good initial guesses to achieve convergence and often produce local minima which leads to undesirable results.

GA is an effective method for solving nonlinear optimization problems and is based on the mechanism of natural selection, in which the stronger individuals are likely to survive in a competitive environment. Here, GA is applied to the SHE-PWM to remove lower order harmonics.

The Fourier coefficients of a periodic signal with symmetry over a quarter of a period and anti-symmetry over half a period are given by:

$$\begin{cases} b_n = 0 \\ a_n = \dfrac{4}{\pi}\displaystyle\int_0^{\frac{\pi}{2}} v_{dc}\sin(n\omega t) \end{cases} \tag{10}$$

For the pulse function of a bipolar voltage, the Fourier coefficients are given as follows:

$$a_n = \frac{4\,v_{dc}}{n\,\pi}\left(\sum_{i=1}^{K}(-1)^{i+1}\cos(n\,\alpha_n)\right) \tag{11}$$

Where v_{dc} is the amplitude of the DC link voltage.

Equation (11) has K equations and n unknowns. K represents the number of switching angles per quarter of a period. Based on this setting, the fundamental component can be controlled and $(K-1)$ harmonics can be eliminated.

To eliminate $(K-1)$ harmonics, one must solve the following system of equations [44, 45]:

$$f(\alpha_i) = \begin{cases} \varepsilon_1 = \frac{4}{\pi}[\cos(\alpha_1) - \cos(\alpha_2) + \cdots \pm \cos(\alpha_K)] - m_i \\ \varepsilon_2 = \cos(3\alpha_1) - \cos(3\alpha_2) + \cdots \pm \cos(3\alpha_K) \\ \vdots \\ \varepsilon_{14} = [\cos(n\alpha_1) - \cos(n\alpha_2) + \cdots \pm \cos(n\alpha_K)] \end{cases} \tag{12}$$

Where m_i is modulation index, the variables ε_1 to ε_{14} are the normalised harmonic amplitude to be eliminated.

The objective function of the SHE-PWM technique to minimize the harmonic content in the line voltage of the inverter and is given by equation (13).

$$f(\alpha_1, \alpha_2, \dots, \alpha_{14}) = \varepsilon_1^2 + \varepsilon_2^2 + \cdots + \varepsilon_{14}^2 \tag{13}$$

The optimal values of the switching angles are obtained by minimizing equation (12) by assigning other constraints of equation (13) and this helps to eliminate some orders of harmonics.

$$0 < \alpha_1 < \alpha_2 < \cdots < \alpha_K < \frac{\pi}{2} \tag{14}$$

The switching angles of the set of nonlinear equations (12) are adjusted to eliminate 13 harmonics (5^{th}, 7^{th}, 11^{th}, 13^{th}, 17^{th}, 19^{th}, 23^{th}, 25^{th}, 29^{th}, 31^{th}, 35^{th}, 37^{th} and 41^{th}) with the first angle being used to control the fundamental of the voltage.

In GA, a set of solutions $(\alpha_1, \alpha_2, \cdots, \alpha_K)$ called population is generated and randomly initialized to guide the algorithm towards the best solution in the search space. During the cooperation phase, the solutions are compared and combined to produce new feasible solutions with the best features.

The cost function $f(\alpha_i)$ is the most important component in the GA and evaluates the fitness of each chromosome. The purpose of this study is to minimize the selected harmonics; therefore, the fitness function must be added to the THD [46].

$$FF_V = \frac{\sqrt{\sum_{j=1,5,7\dots}^{n}\left(\frac{1}{n}\sum_{i=1}^{14}\cos(n\alpha_i)\right)^2}}{\sum_{i=1}^{14}\cos(\alpha_i)} \tag{15}$$

Table 1. GA steps to find the switching angles

The types of algorithm for GA implementation to find the switching angles for various modulation indices are:

i. Start of algorithm

ii. To start the algorithm, look for the number of variables for the specific problem, in our case, the number of variables corresponds to the fourteen switching angles.

iii. The definition of the size of the population with initialization. The population size used was 100 chromosomes. It is assumed that the waveform of the output voltage is symmetrical to a quarter of the frequency, so start the population randomly between the angles 0 and 90°.

The optimal solutions are obtained through several iterations of the objective and fitness functions (equations 12 and 13). Here, the number of iterations is 100 to find the optimal solutions.

iv) The next generation is to determine by fitness values after a first iteration by crossing and mutation, and then a new population is formed.

v) The same evolution is repeated until the solution that satisfies the constraint of equations (14) is reached. Therefore, the inequality constraint equation (16).

Therefore, the inequality constraint of the current SHE problem is expressed as follows.

$$\underbrace{\begin{pmatrix} 1 & -1 & 0 & 0 & 0 & 0 & 0 & 0 & 0 & 0 & 0 & 0 & 0 & 0 \\ 0 & 1 & -1 & 0 & 0 & 0 & 0 & 0 & 0 & 0 & 0 & 0 & 0 & 0 \\ 0 & 0 & 1 & -1 & 0 & 0 & 0 & 0 & 0 & 0 & 0 & 0 & 0 & 0 \\ 0 & 0 & 0 & 1 & -1 & 0 & 0 & 0 & 0 & 0 & 0 & 0 & 0 & 0 \\ 0 & 0 & 0 & 0 & 1 & -1 & 0 & 0 & 0 & 0 & 0 & 0 & 0 & 0 \\ 0 & 0 & 0 & 0 & 0 & 1 & -1 & 0 & 0 & 0 & 0 & 0 & 0 & 0 \\ 0 & 0 & 0 & 0 & 0 & 0 & 1 & -1 & 0 & 0 & 0 & 0 & 0 & 0 \\ 0 & 0 & 0 & 0 & 0 & 0 & 0 & 1 & -1 & 0 & 0 & 0 & 0 & 0 \\ 0 & 0 & 0 & 0 & 0 & 0 & 0 & 0 & 1 & -1 & 0 & 0 & 0 & 0 \\ 0 & 0 & 0 & 0 & 0 & 0 & 0 & 0 & 0 & 1 & -1 & 0 & 0 & 0 \\ 0 & 0 & 0 & 0 & 0 & 0 & 0 & 0 & 0 & 0 & 1 & -1 & 0 & 0 \\ 0 & 0 & 0 & 0 & 0 & 0 & 0 & 0 & 0 & 0 & 0 & 1 & -1 & 0 \\ 0 & 0 & 0 & 0 & 0 & 0 & 0 & 0 & 0 & 0 & 0 & 0 & 1 & -1 \\ 0 & 0 & 0 & 0 & 0 & 0 & 0 & 0 & 0 & 0 & 0 & 0 & 0 & 1 \end{pmatrix}}_{A} \underbrace{\begin{pmatrix} \alpha_1 \\ \alpha_2 \\ \alpha_3 \\ \alpha_4 \\ \alpha_5 \\ \alpha_6 \\ \alpha_7 \\ \alpha_8 \\ \alpha_9 \\ \alpha_{10} \\ \alpha_{11} \\ \alpha_{12} \\ \alpha_{13} \\ \alpha_{14} \end{pmatrix}}_{X} \leq \underbrace{\begin{pmatrix} 0 \\ 0 \\ 0 \\ 0 \\ 0 \\ 0 \\ 0 \\ 0 \\ 0 \\ 0 \\ 0 \\ 0 \\ 0 \\ 0 \end{pmatrix}}_{B} \quad (16)$$

Where X is the parameter vector of the objective function, while A and B are arbitrary constants matrices.

Fig. 6 shows the flowchart of the SHE-PWM switching control signal optimization method based on GA. Using the MATLAB Optimization Toolbox, it is possible to set the constraints on the lower and upper limits for the 14 switching angles, namely 0 and $\pi/2$, respectively [47] and solve the 14 nonlinear equations (12). This process is repeated for the different modulation indices ranging from 0.1 to 2.

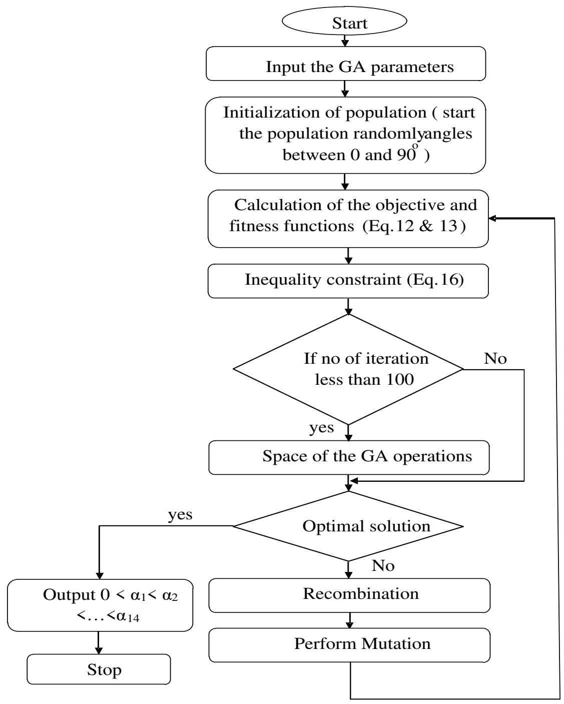

Fig. 6 Flowchart of GA based optimization for the SHE-PWM strategy.

The population size used is 100 chromosomes. It is assumed that the waveform of the output voltage is symmetrical to a quarter of the frequency, so the population is started randomly between the angles 0 and 90°.

The optimal solutions are obtained after 100 iterations of the objective and fitness functions. Fig. 7 shows the trajectory of the commutation angles of the SHE-PWM technique, which are calculated using GA method for modulation indices from 0.1 to 2.

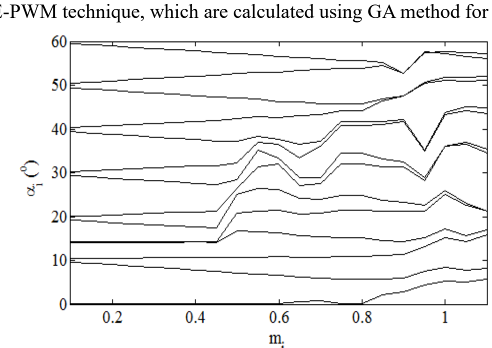

Fig. 7 Trajectory of the optimized switching angles.

These switching angles obtained for a modulation index m_i varied from 0 to 2 are stored in a look-up-table. To generate the

PWM signal, a counter was designed to generate a sawtooth signal as shown in Fig. 8.

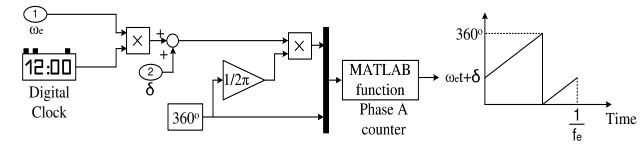

Fig. 8 Switching strategy of SHE-PWM technique.

Fig. 9 represents the block diagram for the calculation of the control laws. These control laws are obtained from the control blocks of the grid-side converter.

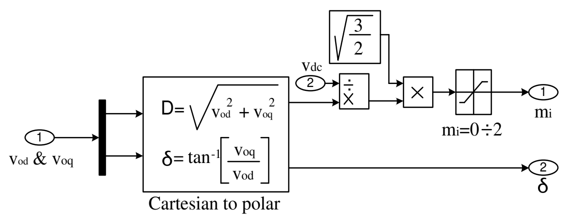

Fig. 9 Calculation of the control signals.

The modulation index m_i obtained by using Fig. 9, is employed to determine the switching angles that are stored in a look-up-table. The generation of PWM control signals is based on the comparison between the optimal switching angles and the sawtooth signal as shown in Fig. 8. This comparison gives the logic state of the grid-side converter switches. This is illustrated for one phase (phase A), the other phases are offset by ± 120°.

5 CONTROL OF THE GENERATOR-SIDE CONVERTER

5.1 Vector control strategy

In general, to find the optimal operating point, the MPPT requires the knowledge of the aerodynamic characteristics of the turbine. However, several MPPT methods determine the operating point without using these characteristics. In this study, the MPPT method employed belongs to the first category.

We introduce a d-q reference frame with an orientation of the rotor flux (d-axis aligned with the direction of the rotor flux). If the frame is perfectly oriented, then:

$$\phi_{rd} = \phi_r, \phi_{rq} = 0 \tag{17}$$

Using Indirect Field-Orientation Control (IFOC) theory and choosing the flux component ϕ_r to be oriented along the d-axis and considering the equations of the fluxes and voltages, the voltages v_{sd} and v_{sq} are obtained as follows:

$$\begin{cases} v_{sd} = \left[R_s + L_s\sigma\frac{d}{dt}\right] i_{sd} - \omega_s L_s \sigma i_{sq} \\ v_{sq} = \left[R_s + L_s\sigma\frac{d}{dt}\right] i_{sq} + \omega_s L_s \sigma i_{sd} + \frac{L_m}{L_r}\omega_s\phi_r \\ T_r\frac{d\phi_r}{dt} + \phi_r = L_m i_{sd} \\ \frac{L_m}{T_r} i_{sq} = \omega_{slip}\phi_r \\ T_e = p\frac{2}{3}\left[\frac{L_m}{L_r}\right]\phi_r i_{sq} \end{cases} \tag{18}$$

Rewriting these equations in steady-state gives:

$$\begin{cases} v_{sd} = R_s i_{sd} - \omega_s L_s \sigma i_{sq} \\ v_{sq} = \omega_s L_s i_{sd} + R_s i_{sq} \end{cases} \tag{19}$$

Similarly, in steady-state, the flux is:

$$\phi_r = L_m i_{sd} \;\; \Rightarrow \;\; i_{sd} = \frac{\phi_r}{L_m} \tag{20}$$

Fig. 10 depicts the IFOC based on the rotor flux orientation scheme for a variable-speed SCIG.

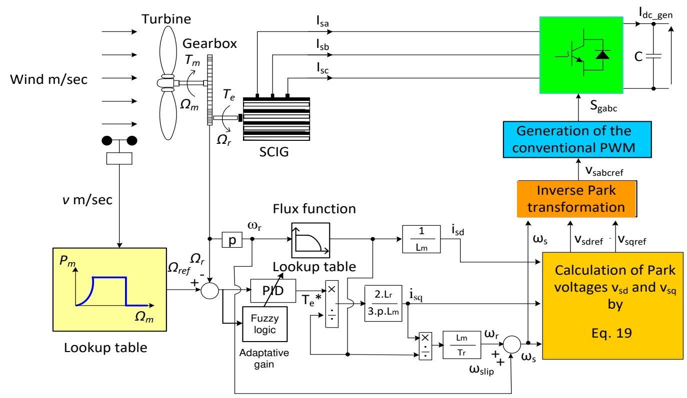

Fig. 10 IFOC of the induction generator.

5.2 Design of the adaptive fuzzy proportional integral derivative controller

The advantage of this controller is that it uses only nine (9) rules and three (3) membership functions which simplifies its implementation and reduces the computation time.

The inputs are the error (e) and its variation (de) and are given by:

$$e(k+1) = \Omega_r^*(k+1) - \Omega_r(k+1) \tag{21}$$

$$de(k+1) = e(k+1) - e(k) \tag{22}$$

The adaption law used to adjust the gains of the PID controller is given by.

$$\gamma(k+1) = \gamma(k) + d\gamma(k) \tag{23}$$

Where k denotes the discrete time.

The output of the adaptive fuzzy PID regulator is the torque T_e used as an input to the IFOC block and is obtained as follows:

$$T_e = \int \gamma\, u(t)dt \tag{24}$$

Where

$$u(t) = K_p e(t) + K_i \int e(t)d(t) + K_d \frac{de(t)}{dt} \tag{25}$$

K_p, K_i and K_d are respectively the proportional, integrator and derivative gains of the PID controller. The structure of the adaptive fuzzy PID regulator is depicted in Fig. 11.

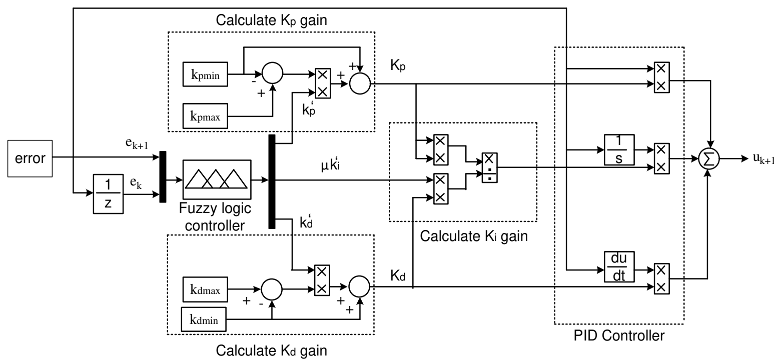

Fig. 11. Structure of the PID regulator with adaptive gains.

The inputs of the fuzzy controller FLC are: the error (e) and the derivative of the error (de), the outputs are; the normalized values of the proportional action k_p', integral action k_i' and derivative action k_d'. the new PID controller parameters are then calculated as follows [48]:

$$K_p = (k_{pmax} - k_{pmin})k_p' + k_{pmin} \tag{26}$$

$$K_i = K_p^2/(\mu\, k_i'\, K_d) \tag{27}$$

$$K_d = (k_{dmax} - k_{dmin})k_d' + k_{dmin} \tag{28}$$

The inputs of the fuzzy controller FLC are: the error e and the derivative of the error, the outputs are; the normalized values of the proportional action k_p', integral action k_i' and derivative action k_d'. The fuzzy sets of the input variables are defined as follows: NB (Negative Big), NM (Negative Medium), NS (Negative Small). Z (Zero), PS (Positive Small), PM (Positive Medium), PB (Positive Big).

The fuzzy sets output variables are defined as follows: L (Large), S (Small).

Memberships functions for inputs and e are defined in the interval [-1, 1] (Fig.12) and the membership functions for the outputs defined in the interval [0,1] (Fig. 13).

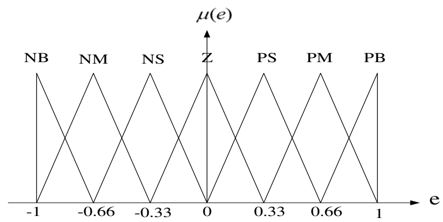

Fig. 12: Membership function for e and de.

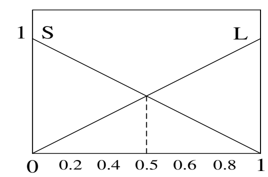

Fig. 13: Membership function of k'_p, k'_i and k'_d.

The rule bases for calculating k'_p, k'_i and k'_d are shown in Tables 2 and 3.

Table 2: Rule base for k'_p

e \ de	NB	NM	NS	Z	PS	PM	PB
NB	L	L	L	L	L	L	L
NM	S	L	L	L	L	L	L
NS	S	S	L	L	L	S	S
Z	S	S	S	L	S	S	S
PS	S	S	L	L	L	S	S
PM	S	L	L	L	L	L	S
PB	L	L	L	L	L	L	S

Table 3: Rule bases for $k'_i$and k'_d.

e \ de	NB	NM	NS	Z	PS	PM	PB
NB	L	L	L	L	L	L	L
NM	L	L	S	S	S	L	L
NS	L	L	L	S	L	L	L
Z	L	L	L	S	L	L	L
PS	L	L	L	S	L	L	L
PM	L	L	S	S	S	L	L

6 SIMULATION RESULTS

The aim of this simulation study is to assess the performance of the proposed SHE-PWM control in improving the overall stability of the WECS. The analysis of the results will focus on: (i) the impact of SHE-PWM control technique on the stability of a WECS in the presence of symmetrical faults, (ii) the influence of the SHE-PWM technique on the energy quality of the system, (iii) use of the gain scheduling controller to further improve the dynamic behavior of the generator. The proposed control schemes will be tested under variable wind speed and three-phase symmetrical faults conditions considering different scenarios.

A. Variable wind speed

The variable wind speed waveform of Fig. 14 is used in this simulation scenario. It can be observed that the wind speed fluctuates between 5 and 12.4 m/s. Fig. 15 shows the responses of the angular velocity of the rotor shaft and the electromagnetic torque developed by the generator. Changes in the speed and the electromagnetic torque of the generator are adapted to the variation of the wind speed of Fig.14.

An increase in the wind speed produces an acceleration of the rotor speed. Fig. 17 shows the responses of the angular velocity. Conversely, reducing the wind speed leads to a decrease in the generator rotor speed as shown in Fig.18.

With this change, the flux in the generator stator is reduced which leads to a decrease in the electromagnetic torque. These results show that a better control of the transient and steady-state responses of the closed-loop system is achieved with the adaptive fuzzy PID controller.

Fig. 16 shows the responses of the real and reactive powers of the system. The powers are directly measured from the electrical quantities. Note that the real power of the grid is negative, and the reactive power is maintained at zero throughout the duration of the simulation to achieve a unity power factor, in other words real power is transferred from the SCIG generators to the grid.

The power variations between -149.2 kW to -10 kW are due to the wind profile shown in Fig. 11. The negative sign of the angle indicates that real power is transferred from the generator to the distribution grid. Fig. 17 shows the DC link voltage and the real and reactive currents in the Park reference frame of the grid. The aim of these controls is to achieve a perfect tracking of the DC bus voltage and the grid currents. The DC bus voltage is controlled around its reference value of 800 V despite fluctuating wind speeds. The real component of the current supplied to the grid follows the variation of the wind speed and the imaginary component is always maintained at its reference value (zero reference).

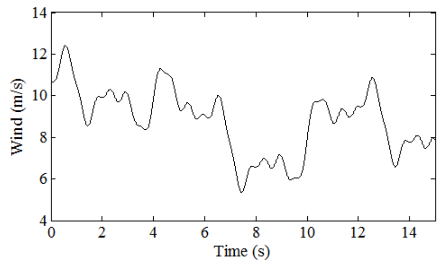

Fig. 14 Wind speed profile.

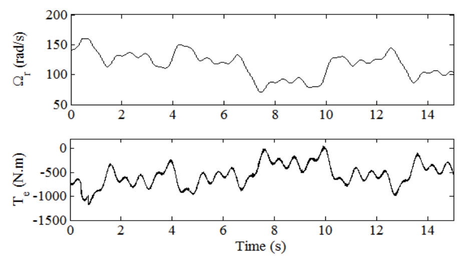

Fig.15 Responses of the angular velocity and the electromagnetic torque of the generator.

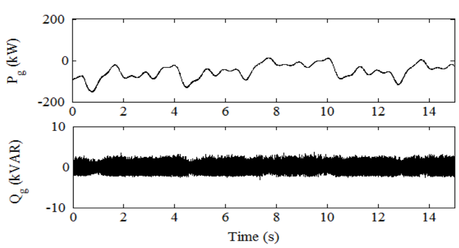

Fig.16 Responses of the real and reactive powers of the grid.

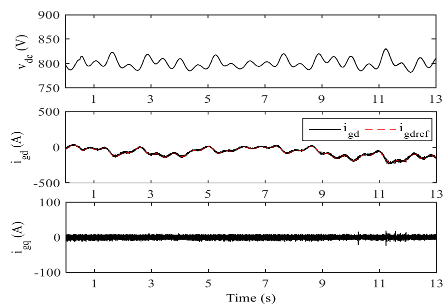

Fig. 17 Waveforms of the DC link voltage and grid currents

B. Symmetrical three-phase fault

B.1 Scenario 1

To assess the influence of voltage dips on the system, a three-phase voltage dip of -20% and +10% with a duration of 1s is applied to the SCIG. Since the duration of the fault is short as compared to wind speed fluctuations, the wind speed was assumed to remain constant during the grid fault and has been set at 11 m/s. Immediately after the fault of +10% applied at $t = 1\ sec$, the voltage increases by 10% as shown in Fig. 18. A transient of the DC bus voltage can be observed.

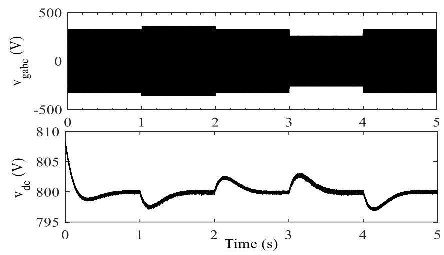

Fig. 18 Waveforms of the grid voltage and DC link voltage during the voltage dip.

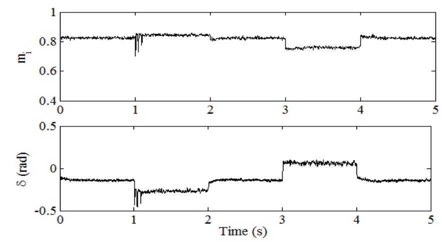

Fig. 19 Control signals of the SHE-PWM.

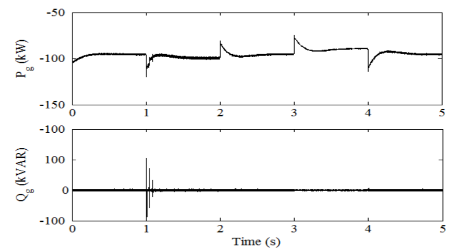

Fig. 20 Responses of the real and reactive powers of the grid.

The modulation index m_i amplitude and phase shift δ are shown in Fig. 19. During the increase of the amplitude of the three-phase voltages of the grid by +10% of its nominal value, a small variation was noticed on the response of the modulation index m_i to maintain the DC voltage constant. In this case, a noticeable change in the phase shift δ with a negative sign can be observed which means that the converter consumes reactive power to ensure zero reactive power in the grid. When the amplitude of the voltage decreased by 20%, m_i is decreased to ensure that the DC voltage is kept at its reference value. In this case the grid requires reactive power that can be generated by the grid-side converter (a positive sign of the phase shift) to maintain a unity power factor. The real and reactive power of the grid during the three-phase symmetrical fault are illustrated in Fig. 20. Note that the reactive power follows its reference of 0 Var throughout the duration of the fault.

B.2 Scenario 2

In this scenario, we performed a comparison between the standard SPWM and SHE-PWM technique optimized by GA under symmetrical three-phase fault simulated as - 50% and +15% voltage amplitude variation. This allows the assessment of the stability range of the two control strategies and test the system around the non-linear region (i.e. with $m_i \approx 1$).

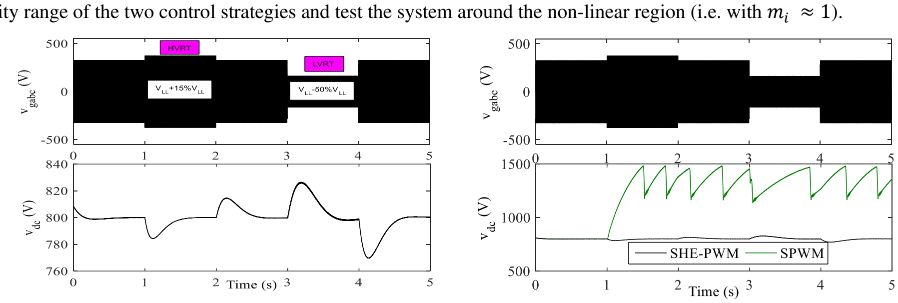

a) SHE-PWM b) SPWM

Fig. 21 Waveforms of the three-phase grid voltage and DC bus voltage.

A symmetrical fault is now applied which is simulated as a decrease (-15%) and an increase (+15%) in the amplitude of the grid voltage as shown in Fig. 21. After the transient, it can be observed that the DC bus voltage follows perfectly the reference in the case of the proposed SHE-PWM technique. On the other hand, oscillations around 1200 and 1500 V (thus ripples of 300 V) were noticed in the case of the standard SPWM control strategy. In addition, the DC link voltage does not follow the assigned reference of 800 V despite the elimination of the fault at times $t = 2\ sec$ and $t = 4\ sec$.

Fig. 22 shows the responses of the rotor speed and the electromagnetic torque of the SCIG generator. A good speed regulation is achieved with the proposed SHE-PWM technique. However, the ripples in the DC voltage caused the response of the speed and torque to quickly deteriorate in the case of the standard SPWM strategy. In this case, the stability range of the proposed technique is wider as compared to that of the classical SPWM due to the ability of SHE-PWM to operate in the nonlinear region (or over-modulation).

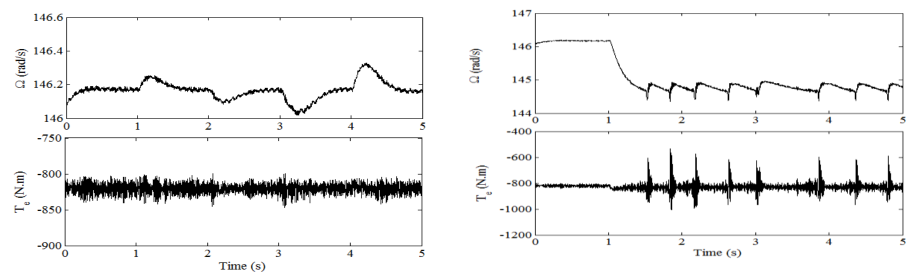

a) SHE-PWM b) SPWM

Fig. 22 Waveforms of the angular velocity and the electromagnetic torque of the generator.

The control signals of the input of the two PWM strategies are illustrated in Fig. 23 (a) and (b). Good stability was obtained with SHE-PWM whereas in the case of SPWM, operation around the nonlinear zone may cause instability. Fig. 24 shows the real and reactive powers of the grid with SHE-PWM and SPWM. In the case of the SHE-PWM technique (Fig. 24 (a)), the real power injected into the grid is almost constant around -100 kW which means that there is a continuous supply of real power to the grid. The reactive power, under all operating condition (without and with fault) follows its reference of 0 Var. In the case of the classical SPWM technique (Fig. 24 (b)), it can be observed that at the onset of the fault the power becomes positive with large ripples which results in a poor energy quality and on the other hand, the grid is now delivering real power to the converter on the DC side. In the case of SPWM, over-modulation and large fluctuations are noticeable in Fig. 23 (b). The instability of the control not only affects the real power, but it also influences the reactive power as the converter on the DC side consumes a large amount of reactive power which causes a reduction in the power factor.

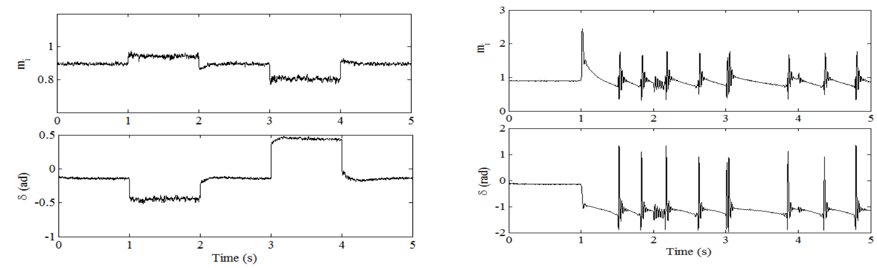

a) SHE-PWM b) PWM

Fig. 23. Control laws

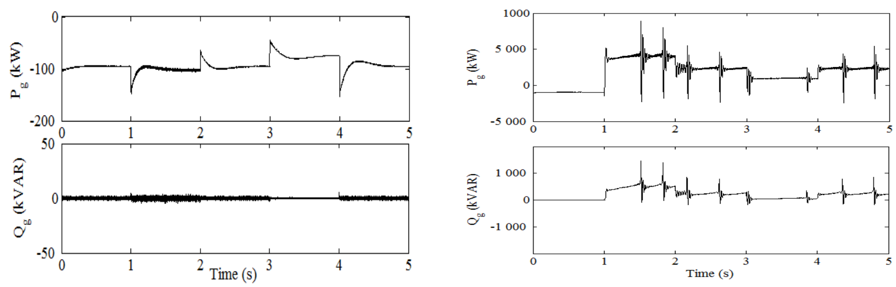

a) SHE-PWM b) SPWM

Fig. 24 Responses of the real and reactive powers of the grid.

B.3 Scenario 3

The aim of this simulation scenario to assess the performance of the proposed control scheme under a severe voltage sag. The voltage was decreased by 80% of the RMS value of the grid voltage. It should be emphasized that this is the maximum fault that can be tolerated under the LVRT grid code requirement of Spain. The voltage sag occurs at time 0.5 s and lasts for 0.5 s. Fig. 25 shows the network phase-voltage waveform under the simulated fault condition.

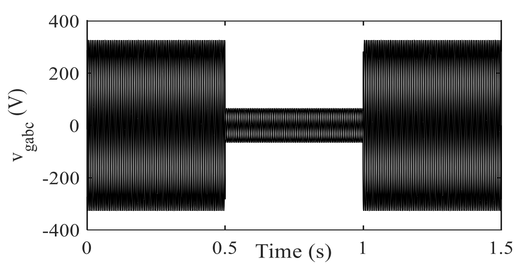

Fig. 25 Network phase voltage waveform under 80 % voltage sag.

Fig. 26 shows the responses of the DC voltage and grid currents in Park reference frame. At the onset of the fault on the grid voltage (voltage sag of 80% of the RMS voltage), the active current of the grid increases in order to ensure cancellation of the reactive current and maintain a unity power factor. The DC voltage follows its reference of 800 V with a small overshoot during the transient regime. The control inputs (the amplitude modulation index m_i and the phase shift δ between the fundamentals of the inverter and grid voltages) are shown in Fig. 27. At the occurrence of the fault, the modulation index m_i is reduced in order to maintain the desired level of DC link voltage. The power flow between the wind energy system and the grid is achieved by adjusting the phase shift δ. Fig. 28 shows the active and reactive powers of the grid side. These results confirm the robustness of the proposed strategy against severe grid voltage drops while ensuring a good energy quality thanks to the SHE-PWM technique based on the genetic algorithm.

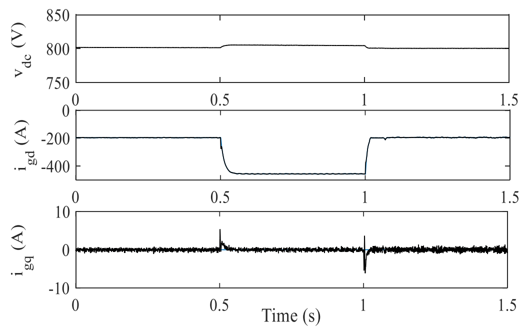

Fig. 26 DC bus voltage and grid currents in Park reference frame

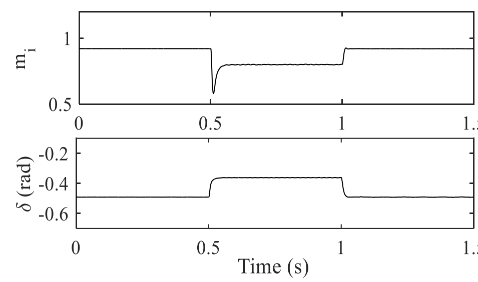

Fig. 27 Control signals.

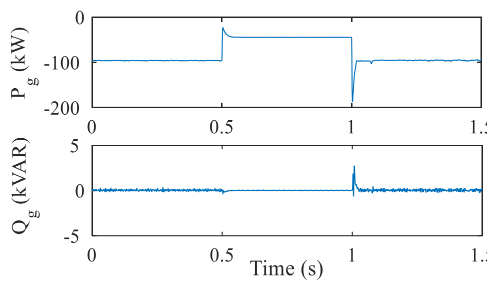

Fig. 28 Active and reactive powers of the grid.

7. CONCLUSION

In this paper a new LVRT and HVRT control method with SHE-PWM optimized by genetic algorithm and an adaptive fuzzy PID controller have been proposed. The behavior of the wind energy conversion system has been investigated under symmetric voltage dips and tested against new LVRT and HVRT grid codes which require wind turbines to remain connected while participating in the restoration of the voltage. The LVRT and HVRT control methods proposed in this paper are based on the use of an SHE-PWM pulse width modulation technique optimized by genetic algorithms to increase the stability range of the DC bus voltage.

The optimized SHE-PWM switching method is proposed for a three-phase, six-pulse inverter circuit topology for a wind energy conversion system. The genetic algorithm-optimized SHE-PWM technique has been used to enhance the quality of the output voltage of the converter. The optimization of the function often requires solving a complex and nonlinear system of equations.

Therefore, calculating online switching angles is almost impossible. In addition, the final solution depends strongly on the initial point. This step could even lead to a non-optimal solution in some cases. For these reasons, we used the MATALB^{TM} Toolbox to calculate these switching angles for different amplitude modulation indexes and to eliminate 13 harmonics (5th, 7, 11th, 13th, 17th, 19th, 23th, 25th, 29th, 31th, 35th, 37th and 41th) with the control of the fundamental of the output voltage. And then these solutions are stored in look-up table and used in the wind energy conversion model.

In addition, an adaptive fuzzy PID controller is proposed to minimize the effect of air turbulence on the wind turbine and to provide good tracking during fluctuating wind speeds.

The simulation results confirmed the effectiveness of the fuzzy adaptive PID control and the superiority of the SHE-PWM strategy over conventional SPWM over the stability margin in the case of symmetrical grid voltage faults.

Data Availability Statement:

Data sharing is not applicable to this article as no new data were created or analyzed in this study.

REFERENCES

[1] G.W.E. Council, GWEC. “Global wind report. Annual market” update 2010; 2011.

[2] CQ Gómez Muñoz, FP. García Márquez, “Wind Energy Power Prospective” Chapter In: Renewable Energies, Springer; 2018. pp. 83–95

[3] Wind Europe, "Wind in Power-2016 European Statistics", Wind Europe Business Intelligence 2017.

[4] S. Djohra, M. Haddadi, and M. Belhamel. “Systèmes décentralisés connectés au réseau électrique : Etude technique, économique et environnementale des systèmes décentralisés connectés au réseau électrique”. Éditions universitaires européennes, 2014.

[5] Y. Yang, W. Chen, and F. Blaabjerg, “, Advanced control of photovoltaic and wind turbines power systems” Advanced and Intelligent Control in Power Electronics and Drives, (2014), 41-89.

[6] L. Hadjidemetriou, E.Kyriakides, Y. Yang and F. Blaabjerg, “A synchronization method for single-phase grid-tied inverters”, IEEE Transactions on Power Electronics, 2016, 31(3), 2139-2149.

[7] Uddin W, Zeb K, Tanoli A, Haider A “ Hardware-based hybrid scheme to improve the fault ride through capability of doubly fed induction generator under symmetrical and asymmetrical fault”, IET Generation Transmission and Distribution, 2018 12(1): 200–206.

[8] Shihabudheen KV, Raju SK, Pillai GN, “Control for grid- connected DFIG-based wind energy system using adaptive neuro-fuzzy technique”, International Transactions on Electric Energy Systems, 2018, 28(5):1–18.

[9] Sid Ahmed El Mehdi Ardjoun, Mouloud Denai, Mohamed Abid, “A robust power control strategy to enhance LVRT capability of grid-connected DFIG-based wind energy systems”, Wind Energy. 2019;1–14.

[10] Muhammad Arif Sharafat Ali, Khawaja Khalid Mehmood, Shazia Baloch and Chul-Hwan Kim, “Modified rotor-side converter control design for improving the LVRT capability of a DFIG-based WECS”, Electric Power Systems Research 186 (2020) 106403.

[11] A. D. Falehi, M. Rafiee, "LVRT/HVRT Capability Enhancement of DFIG Wind Turbine Using Optimal Design and Control of Novel PIλDμ -AMLI Based DVR ", Sustainable Energy, Grids and Networks; Volume 16, December 2018, Pages 111-125.

[12] Rafael M. Silva, Allan F. Cupertino, Guilherme M. Rezende, Clodualdo V.Sousa and Victor F. Mendes, "Power control strategies for grid connected converters applied to full-scale wind energy conversion systems during LVRT operation", Electric Power Systems Research, Volume 184, July 2020, 106279.

[13] C. Zhou, Z. Wang, P. Ju, D. Gan, "A High Voltage Ride Through Strategy For DFIG Considering HVDC System Converter Blocking", Mathematics, Computer Science (2019).

[14] A. Shruthi, "A novel genetic algorithm for selective harmonic elimination in cascade switched diode MLC", International Journal of Advance Research in Science and Engineering, IJARSE, Vol. No.4, Special Issue (02), February 2015.

[15] M. Doumi, A. Aissaoui, M. Abid, A. Tahour, K. Tahir, "Robust Fuzzy Gains Scheduling of RST Controller for a WECS Based on a Doubly-Fed Induction Generator", AUTOMATIKA 57(2016) 3, pp:617–626.

[16] Y. Riffonneau, S. Bacha, F. Barruel, and S. Ploix, "Optimal power flow management for grid connected PV systems with batteries", IEEE Transactions on Sustainable Energy, vol. 2, no.3, pp. 309−320, Jul. 2011.

[17] Z. Shan, S. Yongduan, W. Lei and Z. Zheng, "Neuron-Adaptive PID Based Speed Control of SCSG Wind Turbine System," Hindawi, May 2014, Abstract and Applied Analysis 2014(5):1-10.

[18] Y. Xiuxing, "Hybrid adaptive control for variable-speed variable-pitch wind energy systems using general regression neural network", journal Wind Energ, 24 May 2018.

[19] S.A Taher, M. Farshadnia and M.R. Mozdianfard, "Optimal gain scheduling controller design of a pitch-controlled VS-WECS using DE optimization algorithm", Applied Soft Computing, 2013. 13(5): pp. 2215-2223.

[20] Y. Riffonneau, S. Bacha, F. Barruel, and S. Ploix, "Optimal power flow management for grid connected PV systems with batteries", IEEE Transactions on Sustainable Energy, vol. 2, no. 3, pp. 309¡320, Jul. 2011.

[21] YF Ho, CC Chang, CC Wei, HL Wang, "Multi-objective programming model for energy conservation and renewable energy structure of a low carbon campus", Energy and Buildings Vol. 80, Sept. 2014, pp: 461-468.

[22] F. Filho, L. M.Tolbert, Y. Cao, B. Ozpineci, "Real-time selective harmonic minimization for multilevel inverters connected to solar panels using artificial neural network angle generation", IEEE Trans. Ind. Appl. 2011, 47, 2117–2124.

[23] G. Zhang, J. Yang, Y. Sun, and al, "A Predictive-Control Based Over-modulation Method for Conventional Matrix Converters", IEEE Transactions On Power Electronics, Vol. 33, No. 4, April 2018, pp:3631–3643.

[24] X. Guo, M. He, Y. Yang, "Over-modulation strategy of power converters: A review," IEEE Access, 2018, 6; pp: 69528-69544

[25] A. Hren and F. Mihalic, "An Improved SPWM-Based Control with Over-Modulation Strategy of the Third Harmonic Elimination for a Single-Phase Inverter," Energies 2018, 11,4, 881, pp:1-20

[26] H.L. Fu, H.T. Thien, "Modeling a Wind Turbine System Using DFIG and Realization of Current Control on the Model with Fuzzy Logic Controller", Lecture Notes in Electrical Engineering, Springer, 2014, Vol. 282, pp: 8–92.

[27] P. Ponce, H. Ponce and A. Molina, "Doubly Fed Induction Generator (DFIG) Wind Turbine Controlled by Artificial Organic Networks, Soft Computing, Methodologies and Application, Springer, May 2018, Vol.22, Issue9, pp: 2867-2879.

[28] A. Tamaarat, A. Benakcha, "Performance de la commande des puissances active et réactive dans une éolienne basée sur une MADA", Revue des Energies Renouvelables Vol. 20 N°4 (2017) 635 – 647.

[29] O. Uchechi, J. Peter, W. Linda, R. Angele, "Comparison of two residential Smart Grid pilots in the Netherlands and in the USA, focusing on energy performance and user experiences", Elsevier, Applied Energy 191 (2017) 264–275.

[30] H. Merabet Boulouiha, A. Allali, M. Laouer, A. Tahri, M Denai. A. Draou, “Direct torque control of multilevel SVPWM inverter in variable speed SCIG-based wind energy conversion system”, Renewable Energy 80 (2015) 140–152.

[31] M. Amer Saeeda, H. Mehroz Khana, A. Ashrafb, S. Aftab Qureshia, “Analyzing effectiveness of LVRT techniques for DFIG wind turbine system and implementation of hybrid combination with control schemes”, Renewable and Sustainable Energy Reviews, Volume 81, Part 2, January 2018, pp: 2487-2501.

[32] B. Yeongsu, L. June-Seok, L. Kyo-Beum, “Low-Voltage Ride-Through Control Strategy for a Grid-Connected Energy Storage System”, Appl. Sci. 2018, 8, 57, pp: 1-18.

[33] M. Rahimi and M. Parniani, "Efficient control scheme of wind turbines with doubly induction generators for low-voltage ride-through capability enhancement", IET Renewable Power Generation, Vol. 4, (Issue 3), 242 -252, May 2010.

[34] J. Yang, D. G. Dorrell, J. E. Fletcher, "Fault ride-through of doubly-fed induction generator with converter protection schemes", In Sustainable Energy Technologies, ICSET 2008, IEEE International Conference on, 2008.

[35] Y. EL Karkri, H. EL Markhi, H. EL Moussaou, T. Lamhamdi”, LVRT and HVRT control strategies of Doubly- Fed Induction Generator, J. Electrical Systems 14-4 (2018), pp: 1-20.

[36] D. Zhou and F. Blaabjerg, “Optimized demagnetizing control of DFIG power converter for reduced thermal stress during symmetrical grid fault”, IEEE transactions on power electronics, vol. 33, no. 12, pp. 10326 – 10340, 2018.

[37] M.M. Shabestary,Y. Abdel-Rady I. Mohamed, "Asymmetrical Ride- Through (ART) and Grid-Support in Converter-Interfaced DG Units under Unbalanced Conditions," IEEE Transactions on Industrial Electronics. 2019, Vol. 66, 2.

[38] Z. Hongbo, Y. Liangzhong, W. Weisheng, et al. Outage analysis of large scale wind power under high voltage condition and coordinated prevention and control strategy. Automation of Electrical Power System, 2015, 39(23): 43-48.

[39] L. Shaolin, W. Weisheng, W. Ruiming, et al. Control strategy and experiment research on high voltage ride through for DFIG-based wind turbines. Automation of Electric Power Systems, 2016, 40(16): 76-82.

[40] X. Zhen, Z. Xing, S. Haihua, et al. Variable damping based control strategy of doubly fed induction generator based wind turbines under grid voltage swell. Automation of Electrical Power System, 2012, 36(3): 39-46.

[41] L. Shaolin, Q. Shiyao, W. Ruiming, Y. Xuesong, and D. Linwang,“Study on voltage with stand characteristics and HVRT control strategy for DFIG wind turbines,” in Proc. Int. Conf. Power Syst. Technol. (POWERCON), Nov. 2018, pp. 1183–1189.

[42] LI Ruiqi, H. GENG, G. YANG, “Fault ride-through of renewable energy conversion systems during voltage recovery”, J. Mod. Power Syst. Clean Energy (2016) 4(1):28-39.

[43] EriGrid, “EriGrid Grid Code v5”, EriGrid, 2013.

[44] M. Al-Hitmi, S. Ahmad, A. Iqbal, and al, "Selective Harmonic Elimination in a Wide Modulation Range Using Modified Newton–Raphson and Pattern Generation Methods for a Multilevel Inverter", Energies, February, 2018, 11, 2, pp:1-16.

[45] H. Merabet Boulouiha, A. Allali, M. Denaï, “Grid Integration of Wind Energy Systems: Control Design, Stability, and Power Quality Issues,” Chapter in book, Clean Energy for Sustainable Development, Elsevier 2016.

[46] E. Anandha Banu and D. Shalini Punithavathani, “Real time GA and ANN based selective harmonic elimination in 9 level ups inverter”, ictact journal on soft computing, July 2016, Volume: 06, Issue: 04.

[47] Mohamed Azab and Mohamed A. Awadallah, “Selective harmonic elimination in VSI-fed induction motor drives using swarm and genetic optimization”, Int. J. Power Electronics, Vol. 5, No. 1, 2013.

[48] F. Indra, P. Era, A.W. Novie, "Fuzzy Gain Scheduling of PID (FGS-PID) for Speed Control Three Phase Induction Motor Based on Indirect Field Oriented Control (IFOC)," EMITTER International Journal of Engineering Technology, Vol. 4, No. 2, December 2016.

APPENDIX

Table 3: Parameters of the Simulation Models

Grid	
Effective voltage, V_{LL} [V]	400
Frequency, f_e [Hz]	50
Transformer	
Leakage resistance, R_f [Ω]	0.2
The leakage inductance, L_f [mH]	2
Turbine	
Density area, ρ [kg.m^{-2}]	1.225
Nominal mechanical power, $P_{m,n}$ [kW]	149.2
Radius of the turbine, R [m]	10.5
Nominal wind speed, v_n [m.s^{-1}]	12
Gain of the multiplier, G	17.1806
SCIG	
Nominal power, P [kW]	149.2
Nominal frequency, $f_{g,n}$ [Hz]	50
Stator resistance, R_s [mΩ]	14.85
Stator leakage inductance, L_{ls} [mH]	0.3027
Rotor resistance, R_r [mΩ]	9.295
Rotor leakage inductance, L_{lr} [mH]	0.3027
Cyclic mutual inductance, L_m [mH]	10.46
Inertia, J, [kg.m^{-2}]	3.1
Viscous friction coefficient, f [N.m.s.rad^{-1}]	0.08
Number of pole pairs, p	2
DC-Side Controller	
Proportional gain of DC voltage controller, K_{pdc}	2
Integral gain of DC voltage controller, K_{idc}	100
Source-Side Controller	
Proportional gain of current controller, K_{pc}	6
Integral gain of current controller, K_{ic}	4500
PID regulator with adaptive gains	
$[k_{pmax}, k_{pmin}]$	[1.64 3.07]
$[k_{dmax}, k_{dmin}]$	[1.11 2.1]

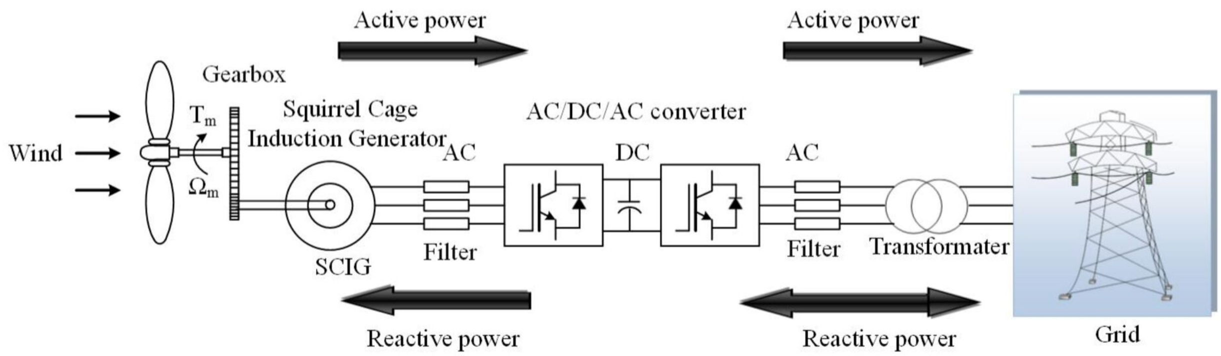

Fig.1 Grid-connected SCIG-based WECS.

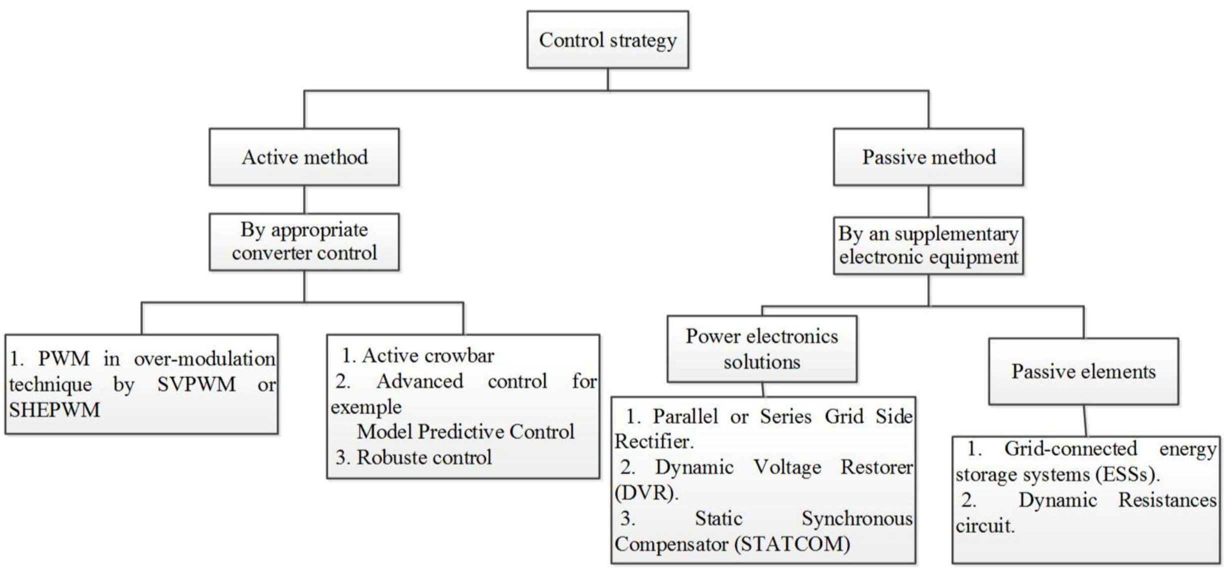

Fig. 2 Control strategies to mitigate grid faults.

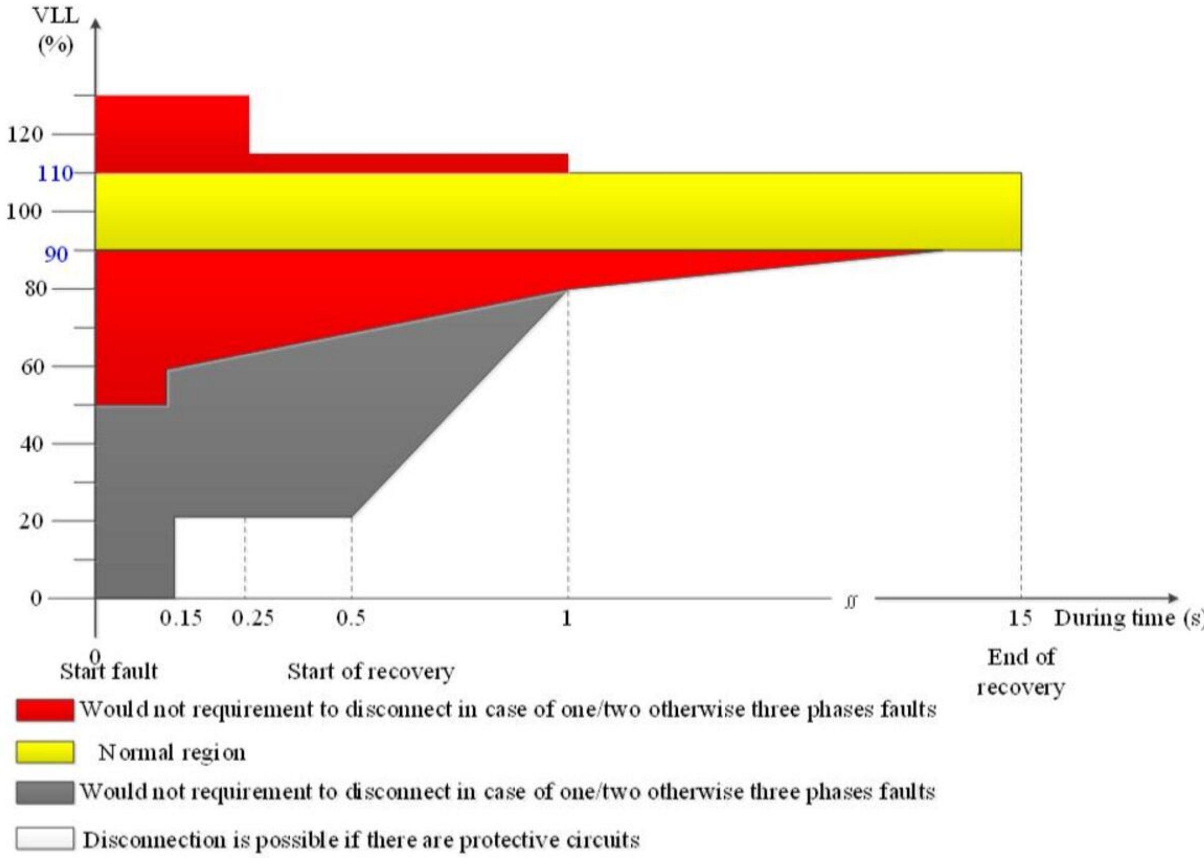

Fig. 3 LVRT and HVRT requirement for the Spanish grid code [36,37].

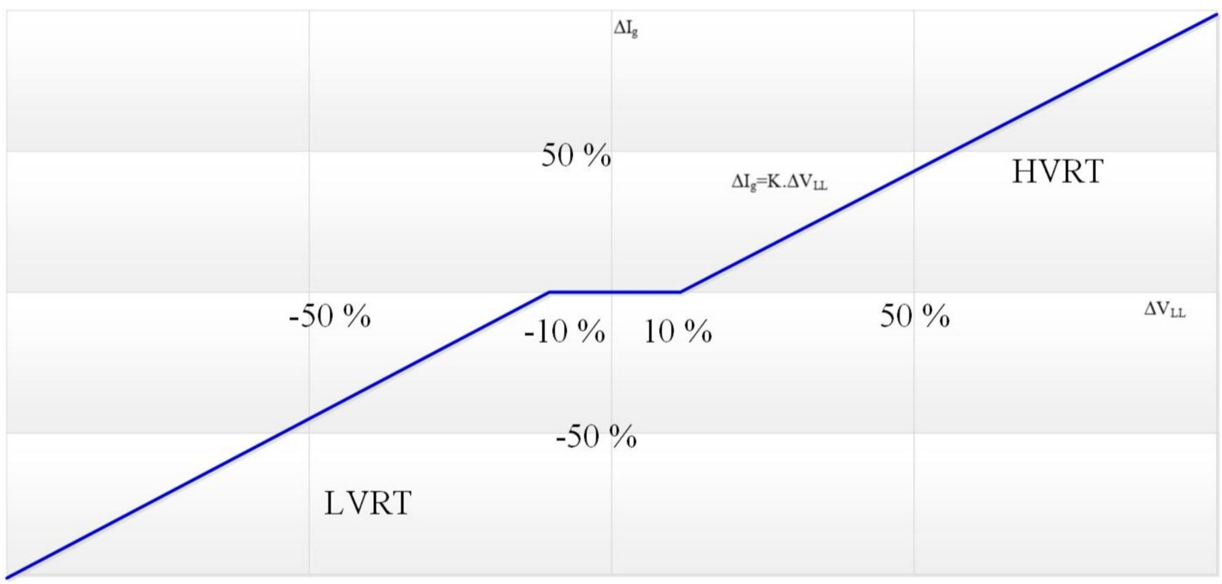

Fig. 4 Reactive current during faults.

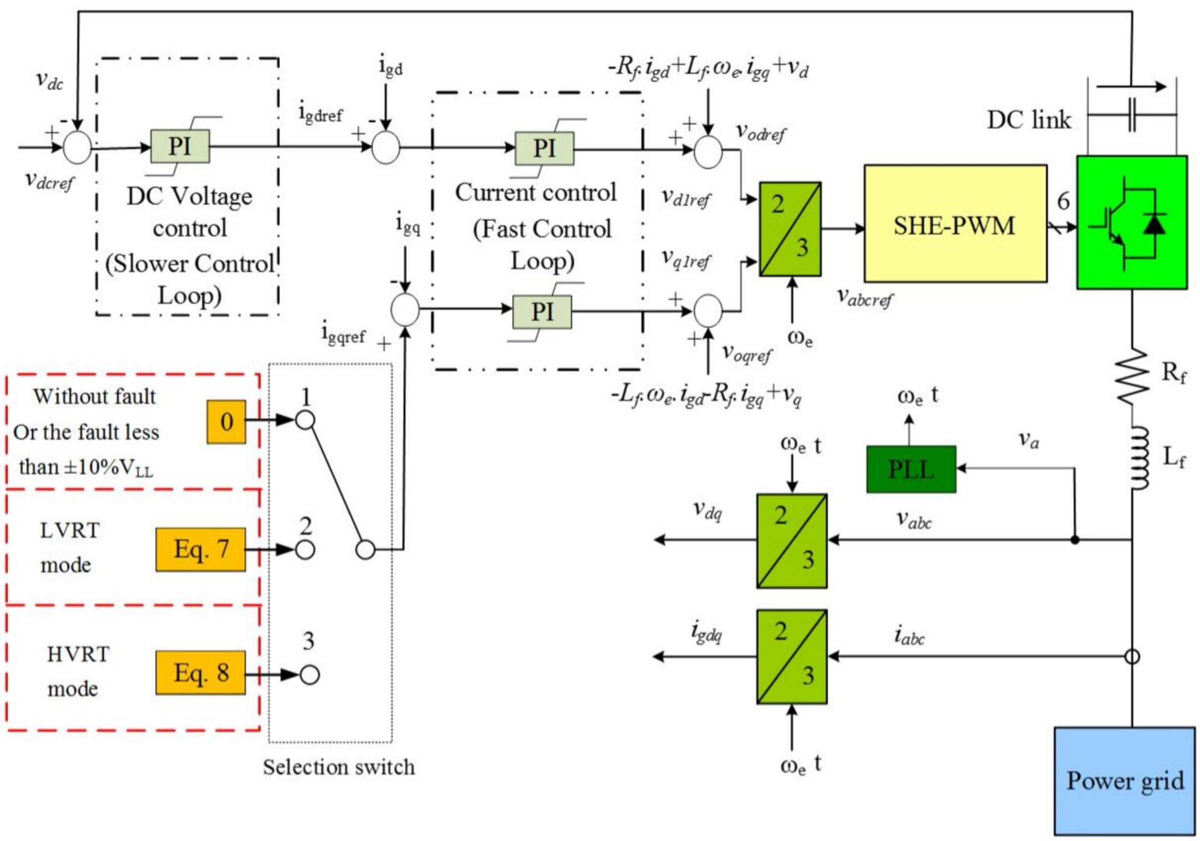

Fig. 5 Control system for the DC link and grid-side.

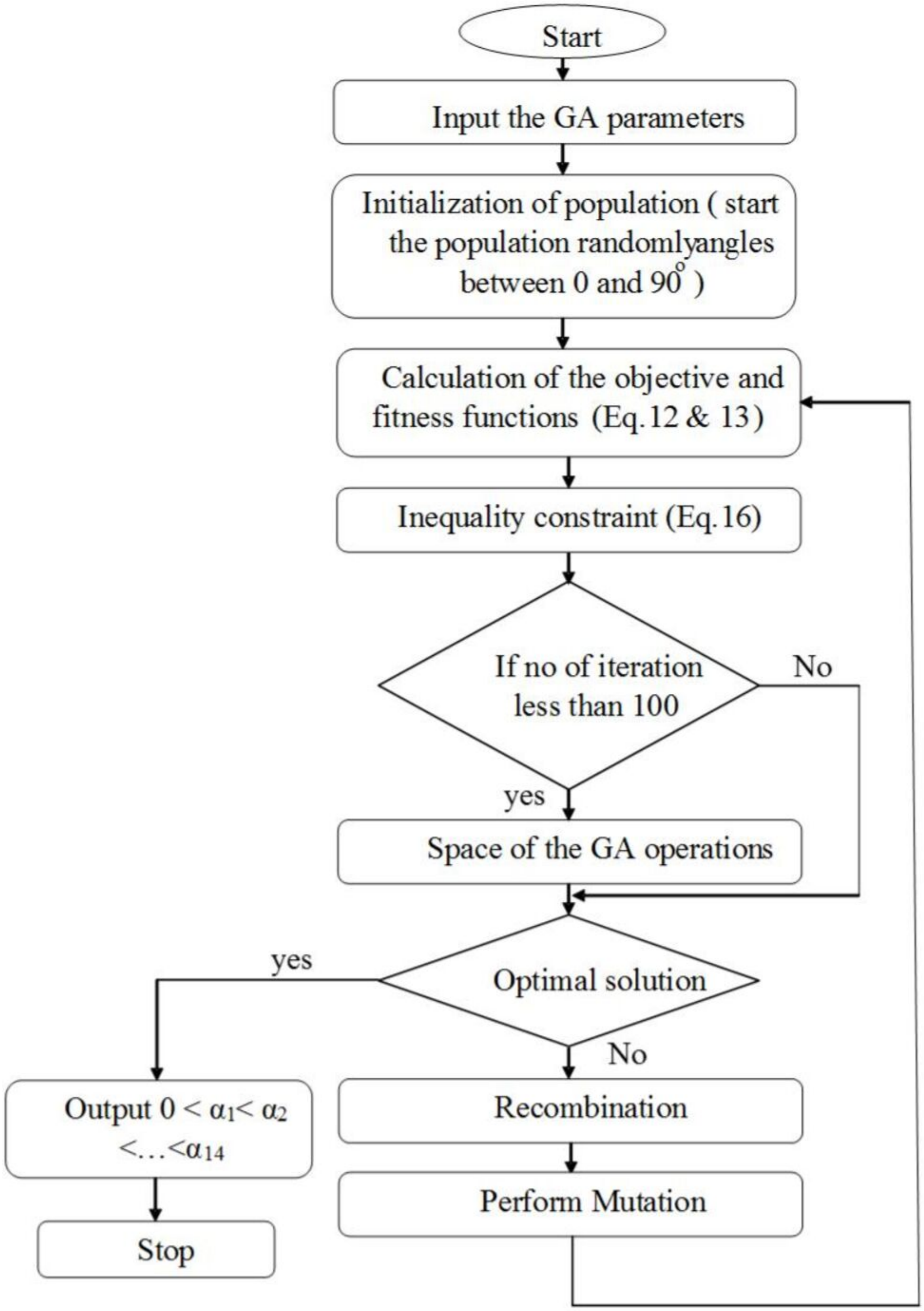

Fig. 6 Flowchart of GA based optimization for the SHE-PWM strategy.

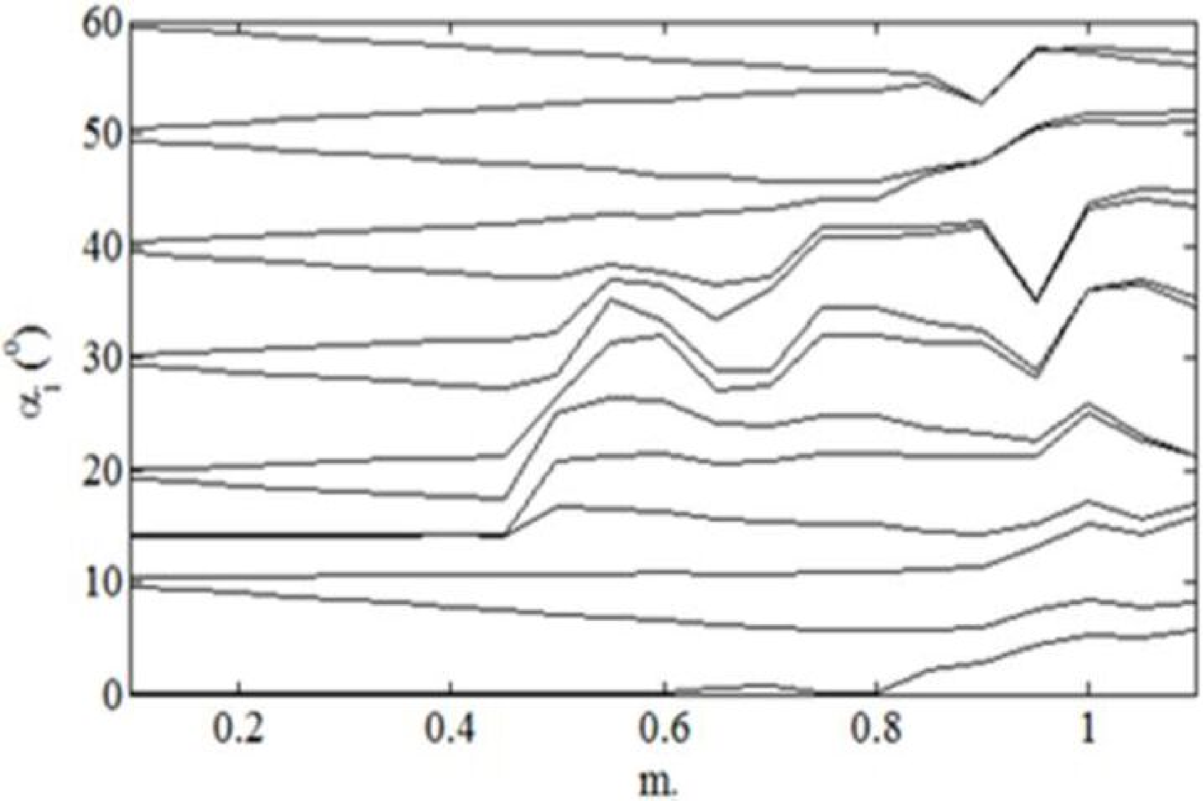

Fig. 7 Trajectory of the calculated switching angles.

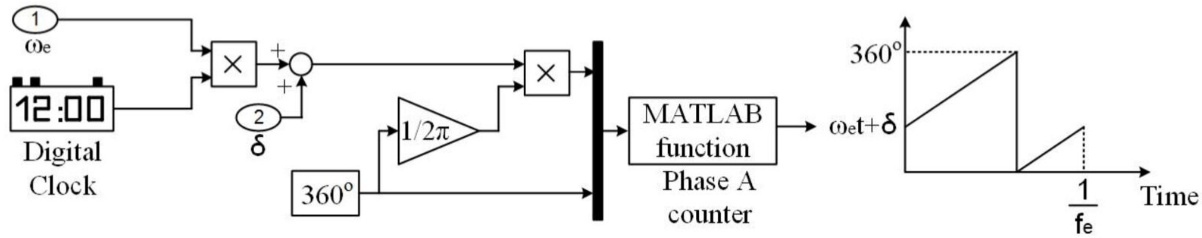

Fig. 8 Switching strategy of SHE-PWM technique.

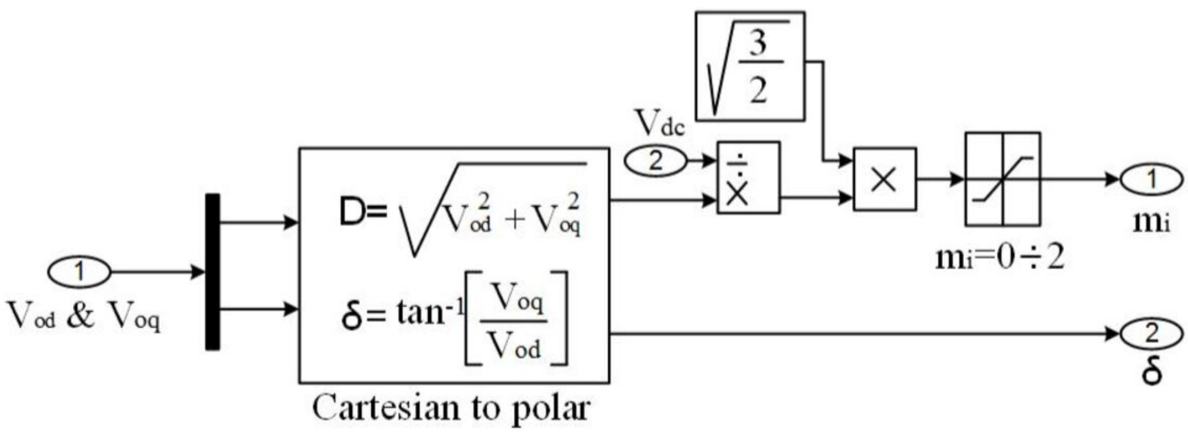

Fig. 9 Calculation control laws.

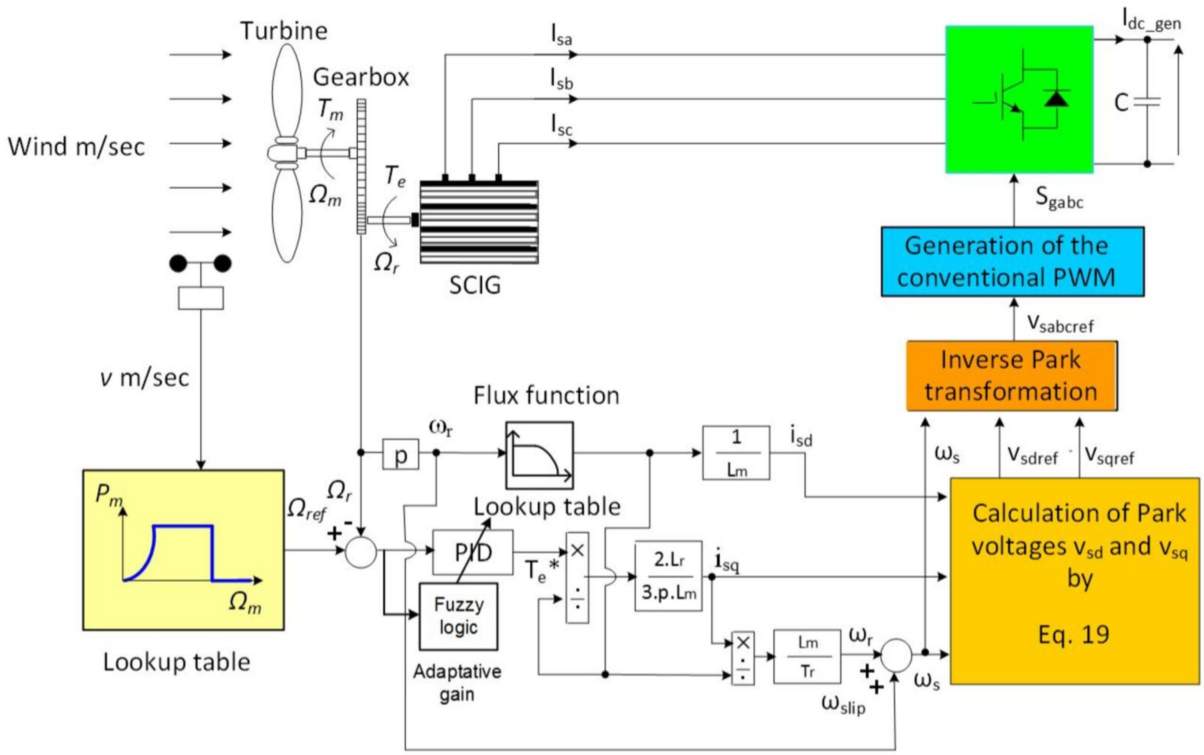

Fig. 10 IFOC of the induction generator.

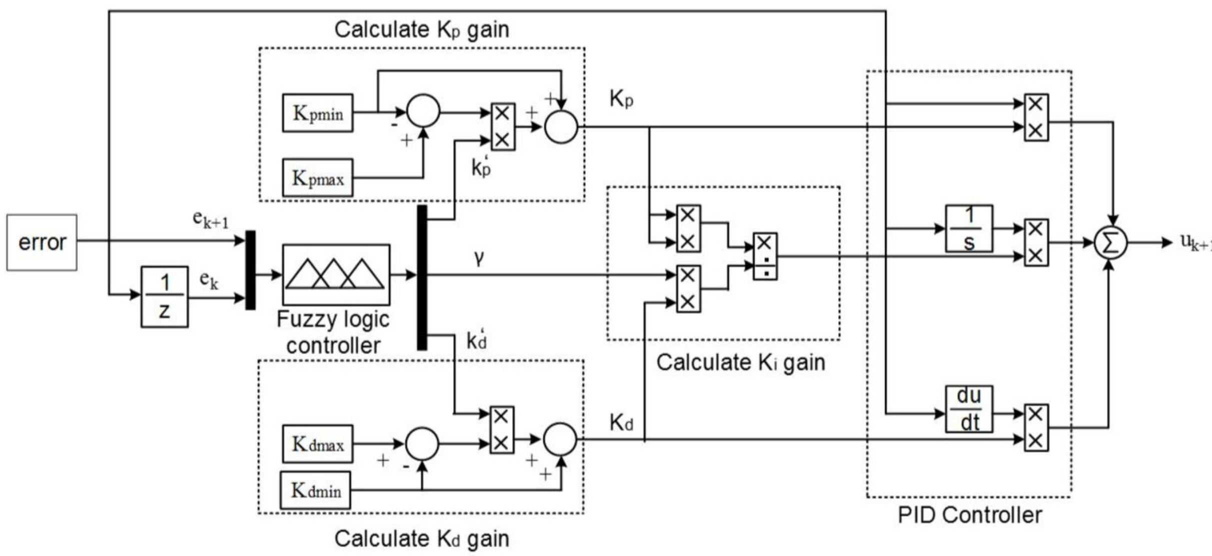

Fig. 11. Structure of the PID regulator with adaptive gains.

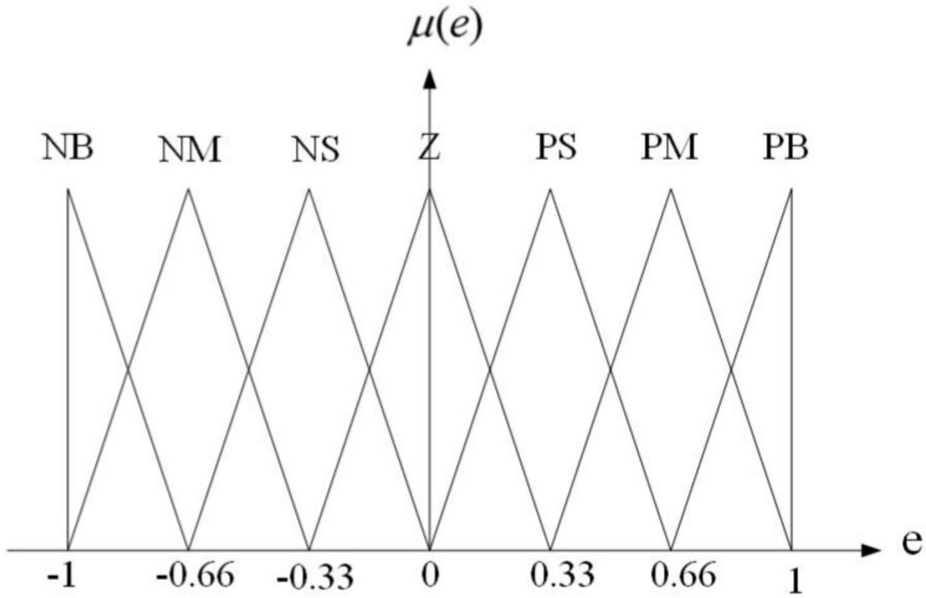

Fig. 12: Membership function for and .Fig. 13: Membership function of e and de .

The rule bases for calculating , *k'p, k'i* and k'd are shown in Tables 2 and 3

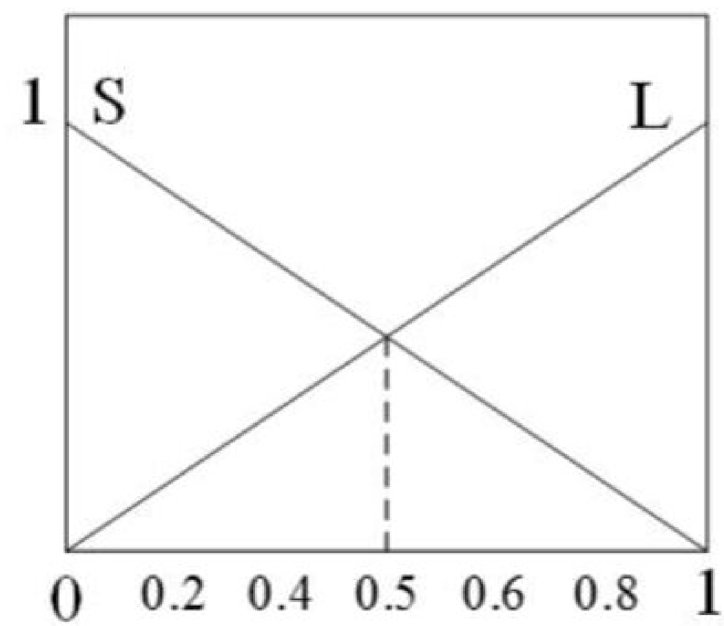

Fig. 13: Membership function of *k'p, k'i* and *k'd*

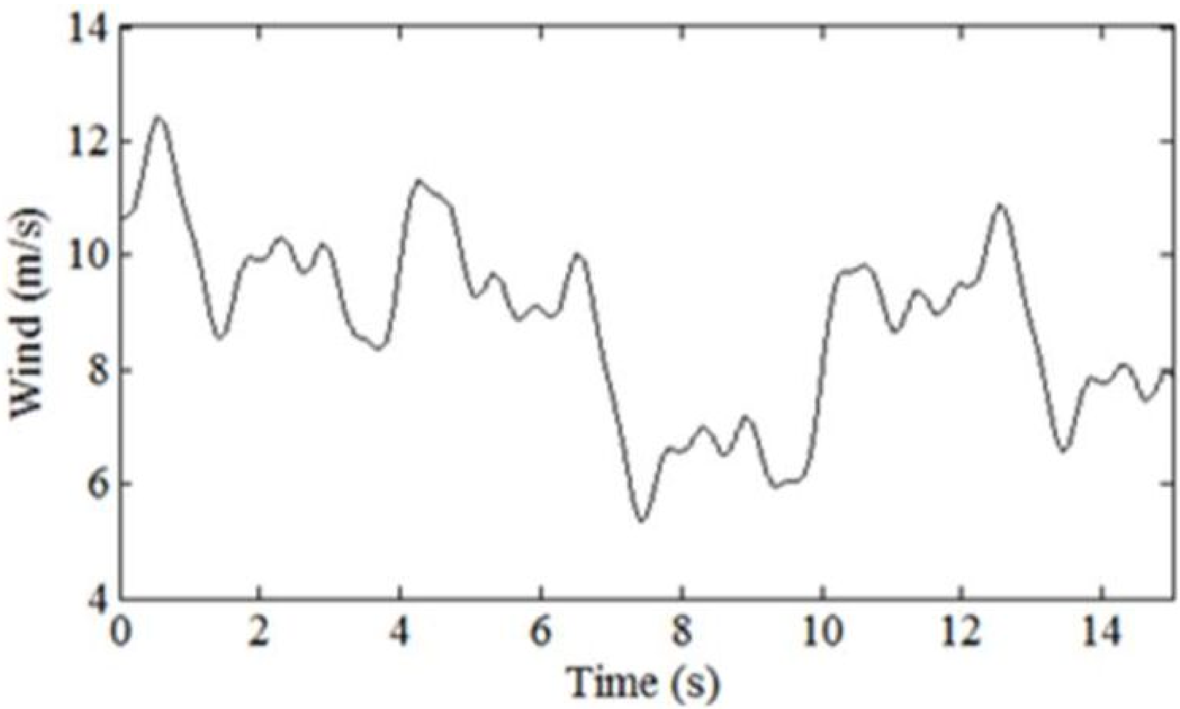

Fig. 14 Wind speed profile

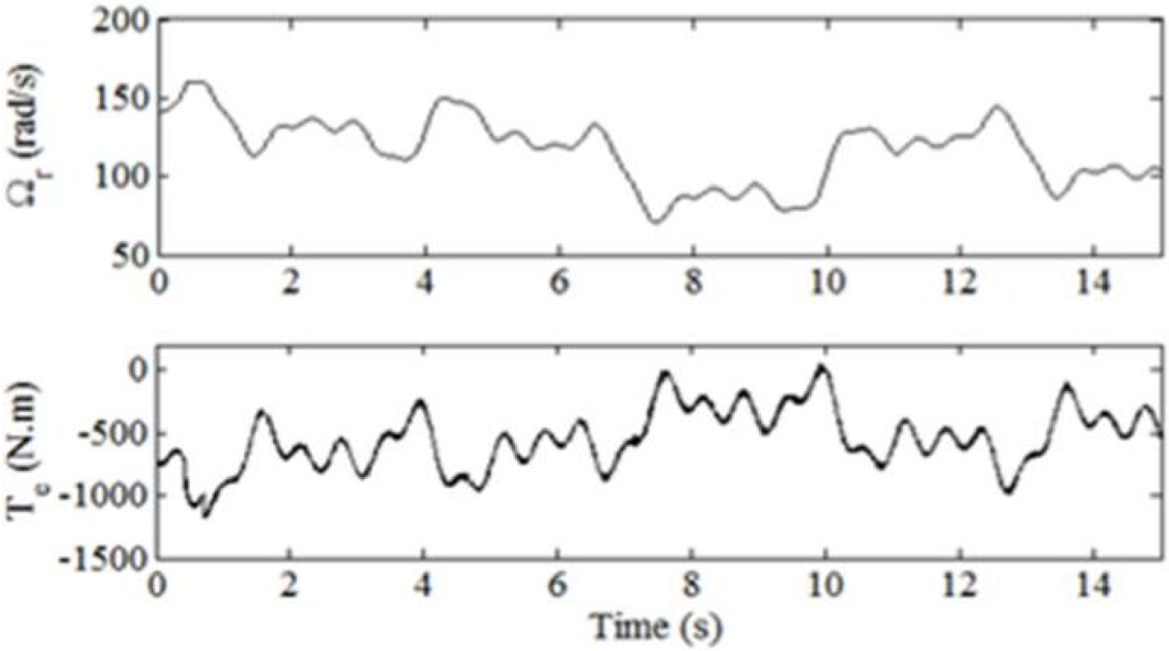

Fig. 15 Responses of the angular velocity and the electromagnetic torque of the generator

PLEASE CITE THIS ARTICLE AS DOI: 10.1063/5.0015579

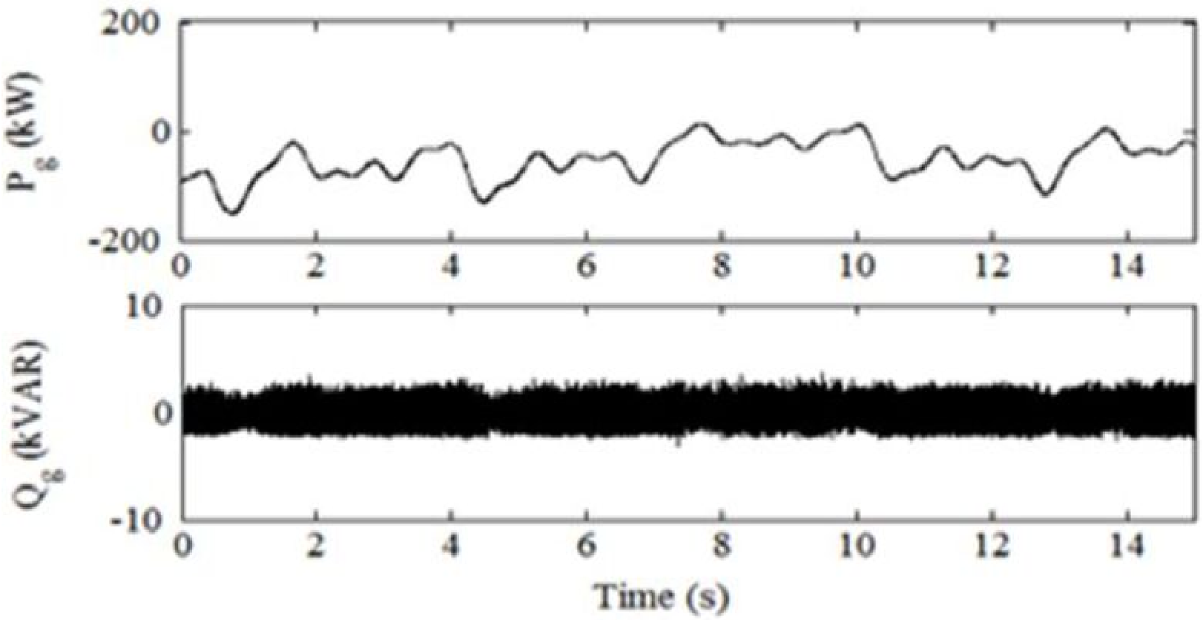

Fig.16 Responses of the real and reactive powers of the grid

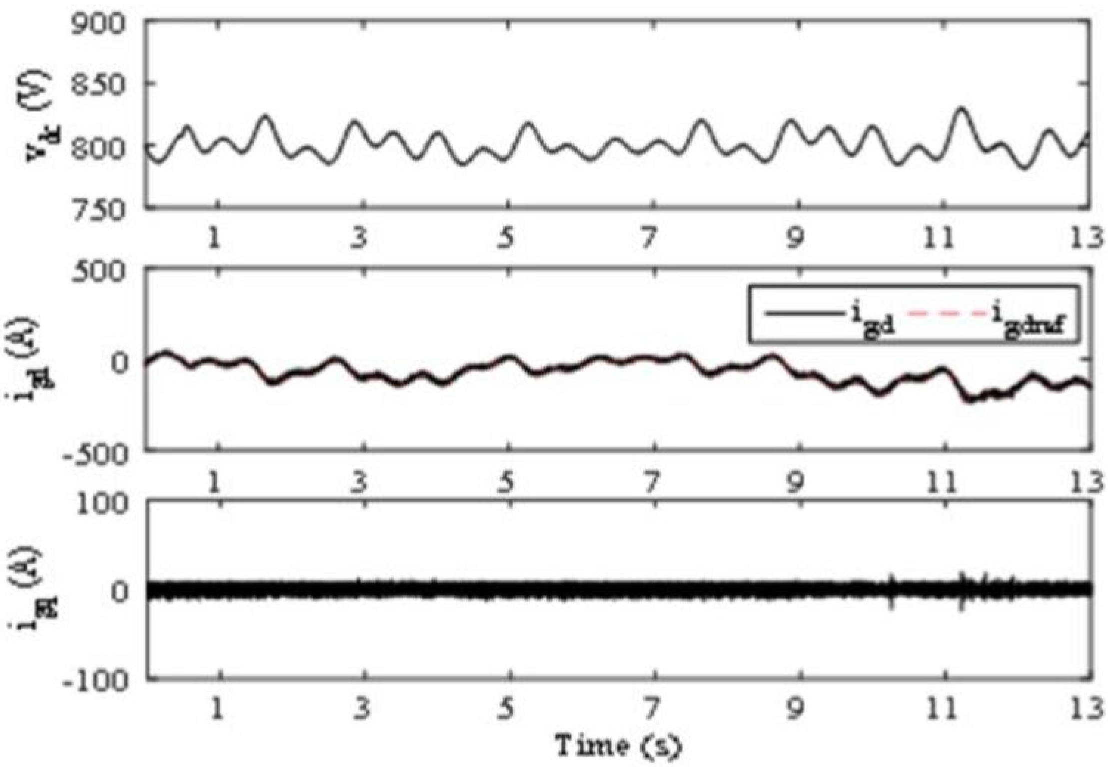

Fig. 17 Waveforms of the DC link voltage and grid currents

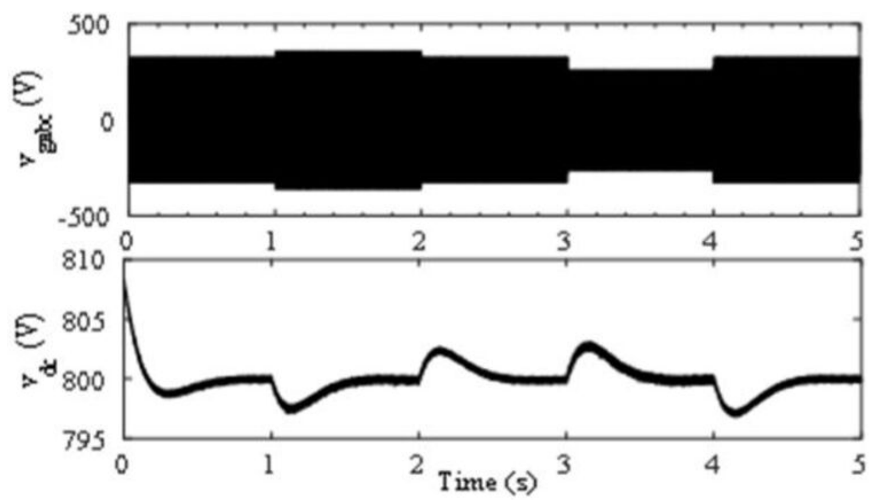

Fig. 18 Waveforms of the grid voltage and DC link voltage during the voltage dip.

PLEASE CITE THIS ARTICLE AS DOI: 10.1063/5.0015579

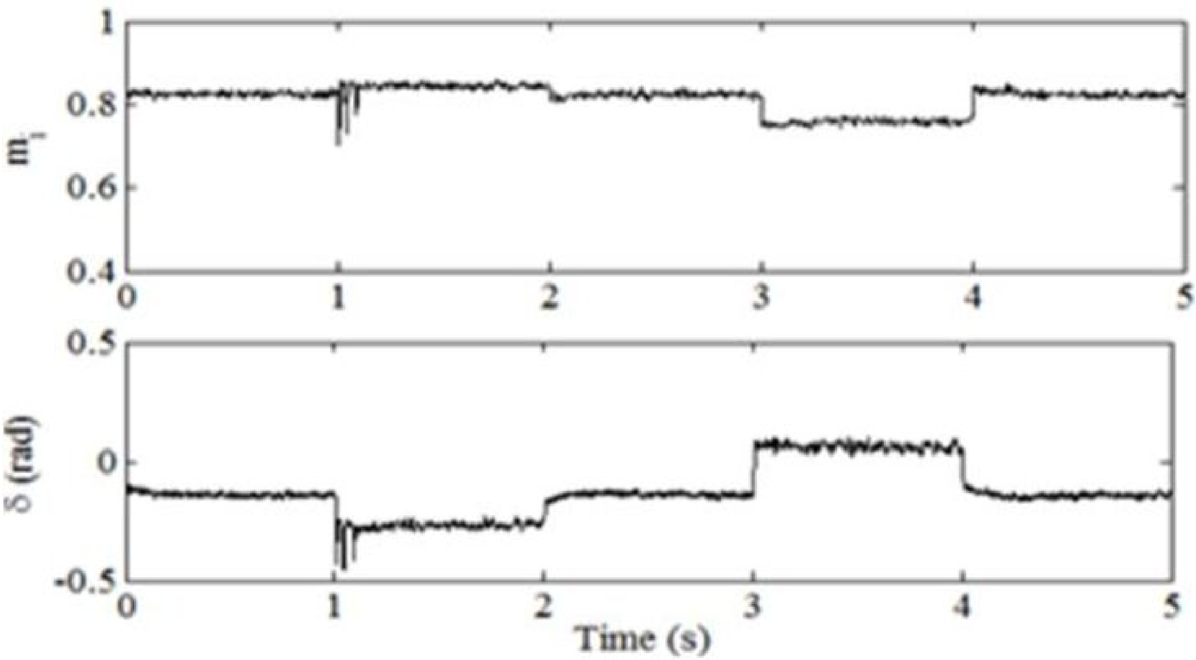

Fig. 19 Control signals of the SHE-PWM.

PLEASE CITE THIS ARTICLE AS DOI: 10.1063/5.0015579

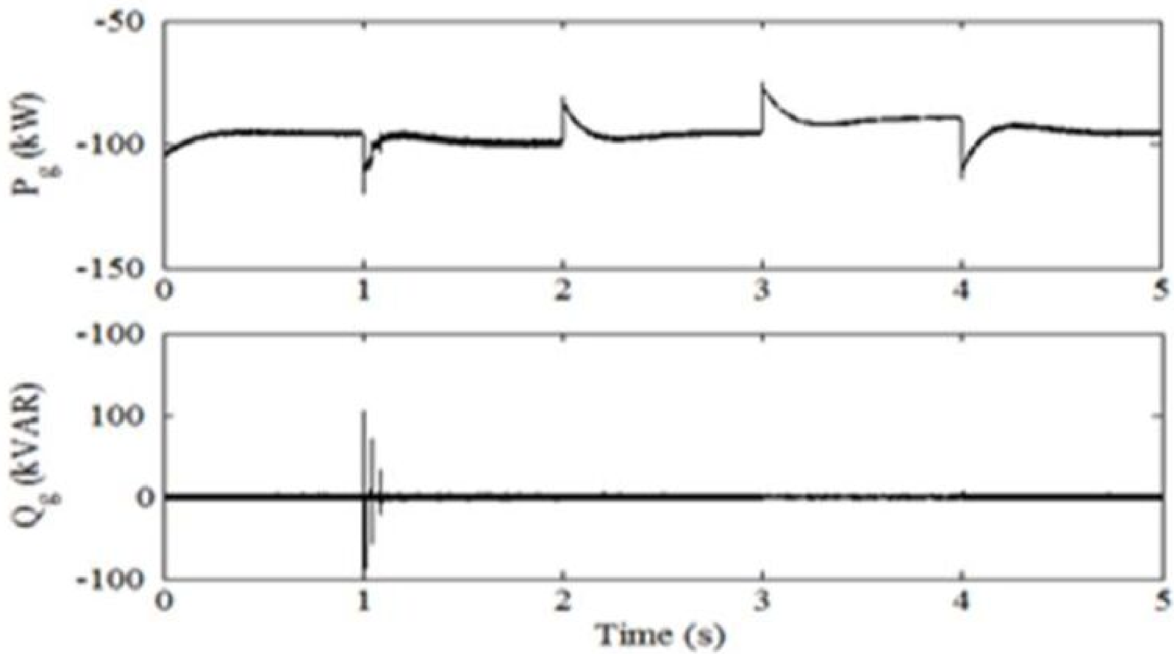

Fig. 20 Responses of the real and reactive powers of the grid.

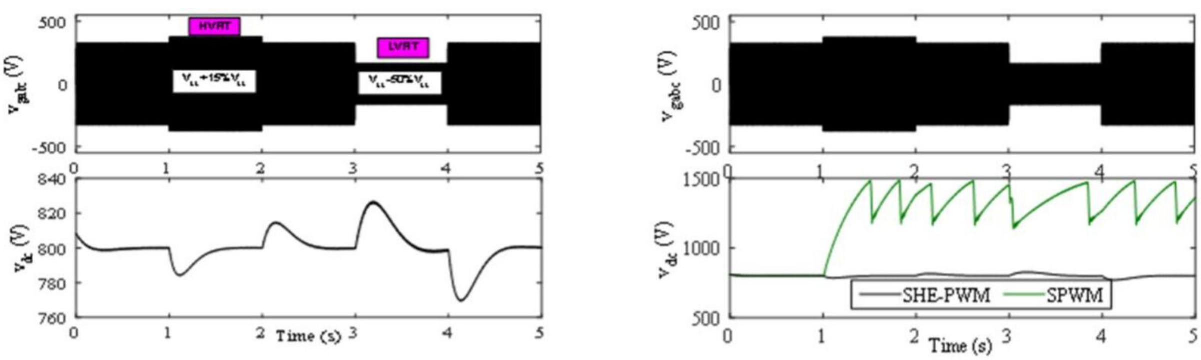

a) SHE-PWM b) SPWM

Fig. 21 Waveforms of the three-phase grid voltage and DC bus voltage.

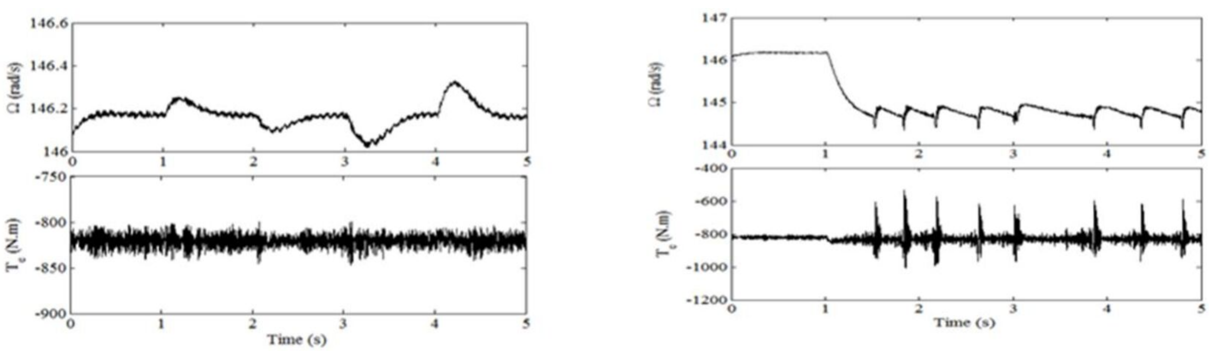

a) SHE-PWM b) SPWM

Fig. 22 Waveforms of the angular velocity and the electromagnetic torque of the generator.

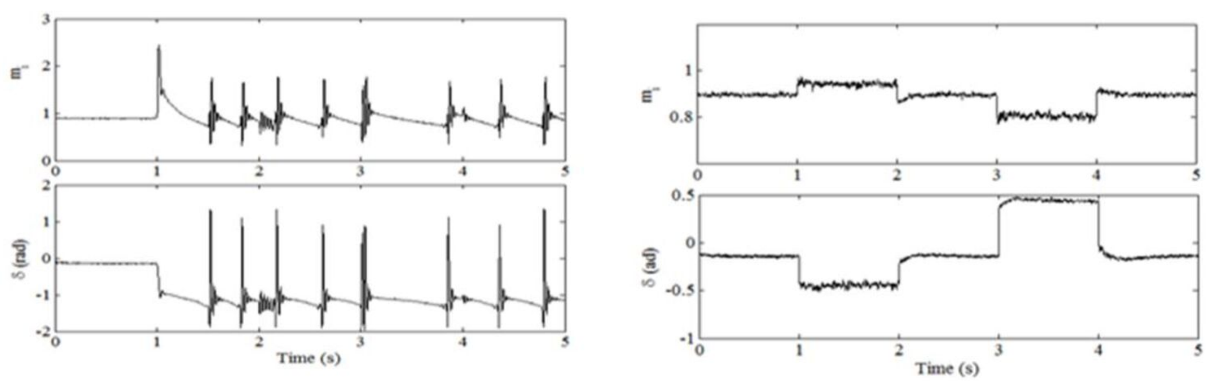

a) SHE-PWM b) PWM

Fig. 23. Control laws

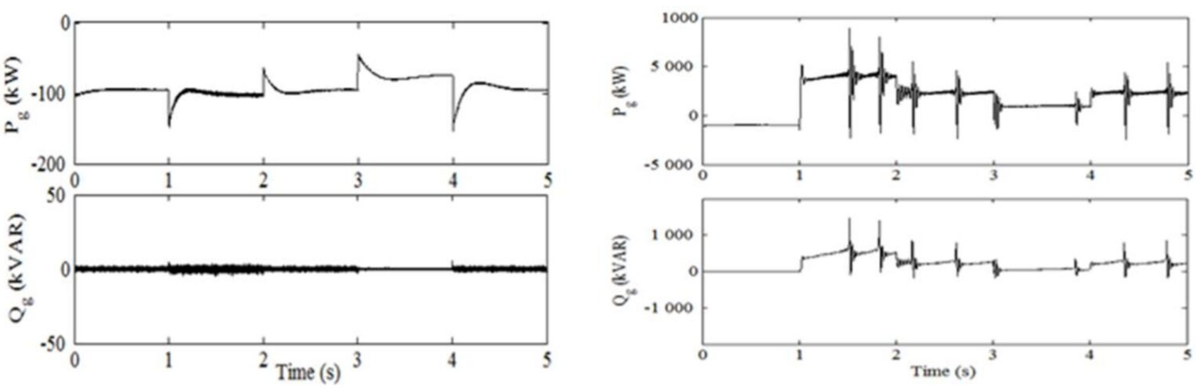

a) SHE-PWM b) SPWM

Fig. 24 Responses of the real and reactive powers of the grid.

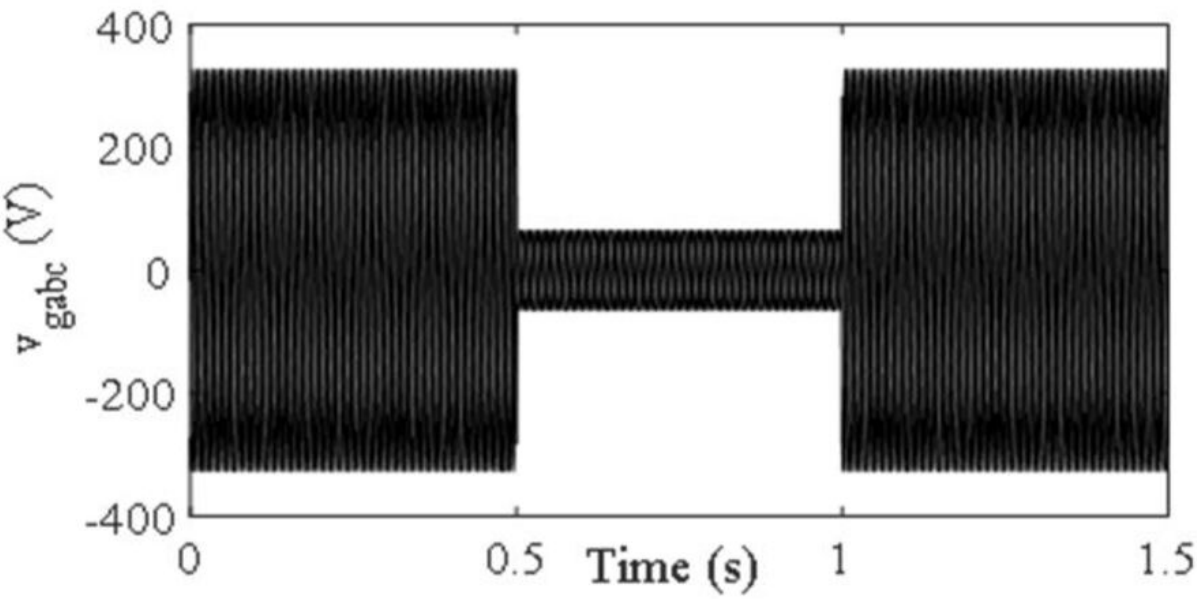

Fig. 25 Network phase voltage waveform under 80 % voltage sag.

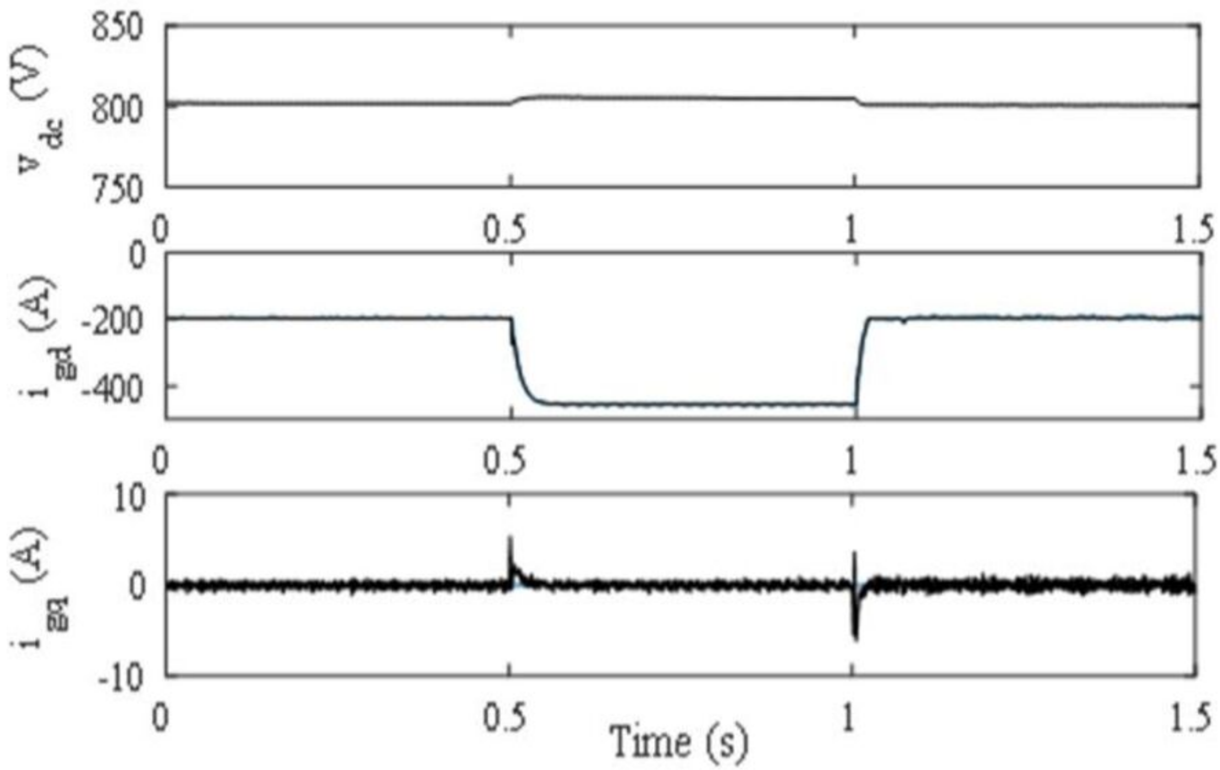

Fig. 26 DC bus voltage and grid currents in Park reference frame

Journal of Renewable and Sustainable Energy

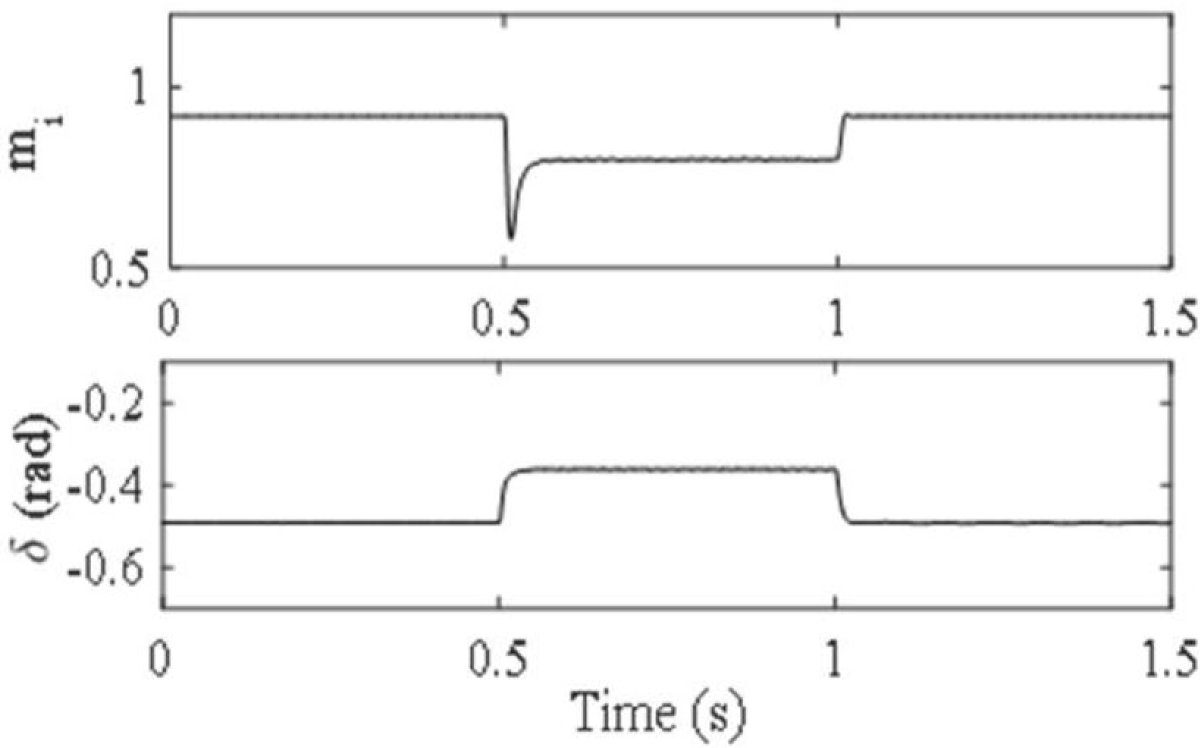

Fig. 27 Control signals.

Journal of Renewable and Sustainable Energy
ACCEPTED MANUSCRIPT

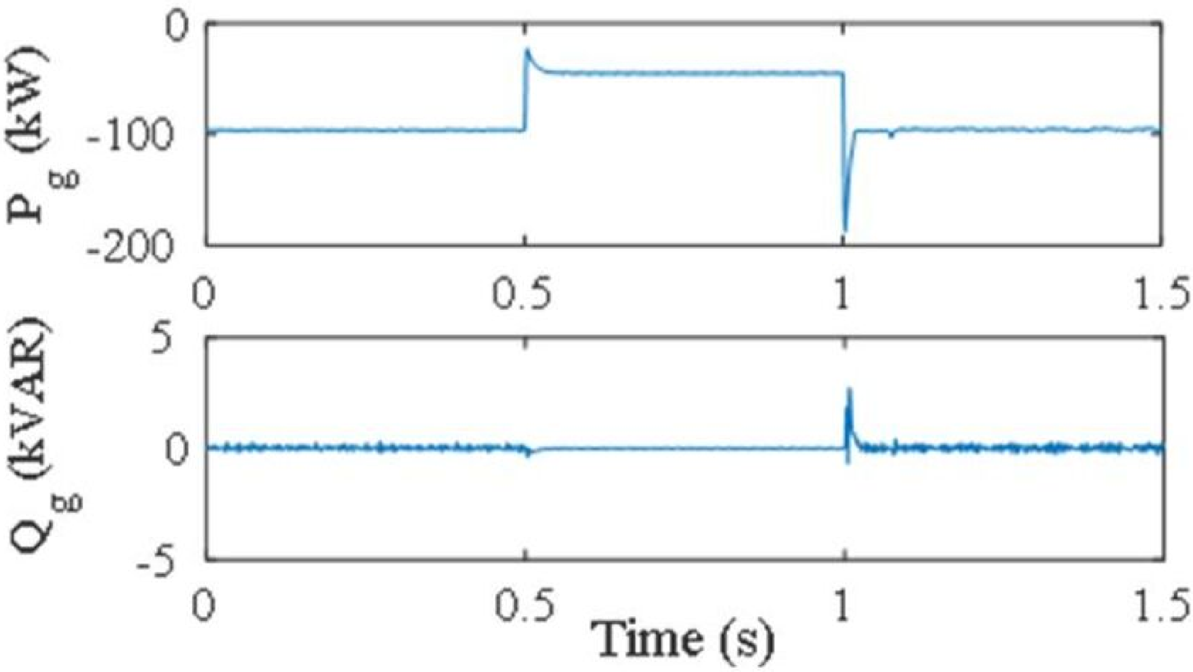

Fig. 28 Active and reactive powers of the grid.